Chemical Engineering Science 318 (2025) 122116

Contents lists available at ScienceDirect

Chemical Engineering Science

journal homepage: www.elsevier.com/locate/ces

Dispersion and residence time distribution of laminar tubular flow in the transition regime – models for flow chemistry and beyond

Martin Wörner

Karlsruhe Institute of Technology (KIT), Institute of Catalysis Research and Technology, Engesserstr. 20, 76131 Karlsruhe, Germany

ARTICLE INFO

Keywords:
Axial dispersion
Continuous flow chemistry
Intermediate regime
Laminar flow
Mixing
Residence time distribution

ABSTRACT

In laminar flow chemistry, tubular reactors are often operated in the transition regime were neither the axial dispersion model nor the pure convection model are valid. This paper presents for solute transport under Poiseuille flow models for the residence time distribution (RTD) in the transition regime missing previously. A novel approach uses an assumed outlet concentration field to calculate the RTD fully analytically via the mixing cup average concentration and its moments. The proposed mechanistic transition regime model (MTR model) depends on the time scale ratio of transversal diffusion and space time as sole parameter, is predictive for straight tubes and recovers the pure convection and axial dispersion models in the limits. In addition, a simplified compartment model based on a plug flow reactor followed by tanks-in-series is proposed (dTiS model). In combination with a correlation for a dispersion reduction factor, both models are predictive for coiled tubes and can be used for reaction engineering design. They are also useful to predict or characterize RTDs in other applications, as demonstrated for a pneumatic flotation cell.

1. Introduction

1.1. Continuous flow chemistry

Chemical engineering can contribute in a number of ways to achieving the 17 sustainable development goals set by the United Nations in 2015 by 2030 (Aristizábal-Marulanda et al., 2024) and beyond (Bollini et al., 2023). In production, sustainability essentially requires making the best use of educts by maximizing yield while reducing waste and energy consumption, a goal which may be achieved for many processes by applying continuous flow chemistry (Plutschack et al., 2017) instead of batch reactors. In continuous flow chemistry (CFC), a chemical reaction is run in a continuous stream flowing through channels or tubing. While operation in batch mode (e.g. in stirred tanks) has its own benefits (Holtze and Boehling, 2022), CFC offers some major advantages as compared to batch production. Besides faster and safer reactions in drastically reduced reactor sizes, these include improved control over temperature and product quality, cleaner and more sustainable products, and the integration of typically separate processes such as synthesis (Hartman and Jensen, 2009), work-up and analysis. To obtain full benefit of CFC in reaction technology, it should be combined with integrated product and process design based on a fundamental understanding of reactors and reactions (Agar et al., 2023). One problem in this context is dispersion, which is the process whereby a locally concentrated solute is distributed in a solvent toward the equilibrium condition of uniform concentration (Probstein, 1994). In CFC, the pipe diameter is usually small resulting in laminar flow. While dispersion in laminar flow reactors is largely understood, it is not modelled properly in the transition regime (also called intermediate regime) where both, transversal diffusion and longitudinal convection determine solute transport.

1.2. Dispersion

The effects on solute transport resulting from the combined action of molecular diffusion and the non-uniform axial velocity in a shear flow are known as Taylor-Aris dispersion (Aris, 1956; Taylor, 1953). This type of axial dispersion is a key phenomenon in reactor engineering that can affect yield and selectivity when reactions are carried out in empty or packed bed tubular reactors. While large dispersion can create concentration gradients that may be useful for studying biochemical reactions (Wang et al., 2017), low dispersion is desirable in purification and separation applications (Datta and Ghosal, 2009) such as on-chip capillary electrophoresis (Bharadwaj et al., 2002) and chromatography where it contributes to extra-column band broadening (Desmet and Broeckhoven, 2019). In flow injection analysis as an automated

E-mail address: martin.woerner@kit.edu.

https://doi.org/10.1016/j.ces.2025.122116
Received 17 January 2025; Received in revised form 30 May 2025; Accepted 25 June 2025
Available online 26 June 2025

approach to chemical analysis (Hansen and Miró, 2007), a bolus of a chemical sample is injected into the flowing carrier stream; this bolus takes on different shape as it disperses downstream depending on the parameters of the system.

Beside chemical engineering and chemistry, shear dispersion theory has application to a number of other fields including material science (continuous production of nano-materials and catalyst), food industry (continuous thermal processing of liquid foods (Torres and Oliveira, 1998), pasteurization of milk in holding tubes (Gutierrez et al., 2010)), live sciences (continuous production of pharmaceuticals and bio-pharmaceuticals, continuous virus filtration (Chen et al., 2024)), biology (nutrient transport in blood vessels, active swimming micro-organisms (Peng and Brady, 2020)) and environmental fluid mechanics (spreading of pollutants and contaminants in porous groundwater aquifers, rivers (Young and Jones, 1991), estuaries (Chatwin and Allen, 1985) and constructed wetlands for treating waste-waters from domestic and industrial sources (Werner and Kadlec, 2000)). The understanding, quantification and proper modeling of the dispersion of dissolved substances in flowing streams is thus of importance for a plethora of applications.

Physically, dispersion of soluble matter in a solvent flowing laminar with mean linear velocity U through a straight circular pipe (inner radius a, inner diameter $d = 2a$, length L, cross-sectional area $A = \pi a^2$) arises due to the interaction of longitudinal advection and transverse molecular diffusion resulting in the exchange of solute between the fast-moving fluid near the center and the slow-moving fluid near the wall. Accordingly, the degree of dispersion is characterized by the competition of two time scales. The time scale of longitudinal advection is the space time $\tau_s = L/U$, representing the mean (or average) residence time of the solvent. The time scale of transversal (radial) diffusion is $\tau_d = a^2/D$, where D denotes the molecular diffusion coefficient of the solute (tracer) which is assumed constant independent of concentration. We indicate the ratio between both time scales by $\alpha = \tau_d/\tau_s = a^2U/LD$. The models developed in this paper are formulated as a function of α only.

1.3. Residence time distribution

Mixing happens at different scales. The mixing being associated to the flow regime and flow patterns within the reactor and occurring over the entire reactor volume is characterized by the residence time distribution (RTD). The residence time is defined as the time that a material element needs to proceed from an inlet of an apparatus or system to its outlet. Because different elements follow different paths, there will be a spread on the residence time. The distribution of residence time is usually determined by an input-response experiment. The differential residence time distribution $E(t)$ defines the probability that a fluid elements spends a total time t in the reactor; it is particularly useful to quantify the deviation from ideal plug flow. Time integration of $E(t)$ yields the cumulative residence time distribution $F(t)$ representing the fraction of the solute that has spent in the system a time t or less. To allow for a better comparison of different residence time distributions, each residence time distribution is usually normalized, either by its mean value or more common by the space time of the reactor. The concept of RTD for the analysis of chemical reactors was first introduced by Mac Mullin and Weber (1935) and worked out in more detail for continuous flow systems and laminar pipe flow by Danckwerts (1953). The main advantage of the RTD is that it allows understanding the flow behavior of the system by concentration measurements at the outlet without having to account for the complete history of each fluid element inside the reactor. While traditionally developed for liquid-based systems, the RTD concept is also applied for gas flows in microreactors (Wibel et al., 2013) and for processing of solids (Gao et al., 2012), with applications ranging from powders to granular systems like pharmaceuticals (Bhalode et al., 2021). The status of RTD theory is frequently reviewed (Nauman, 1981, 2008; Nechita et al., 2023; Rodrigues, 2021; Wen and Fan, 1975).

The development of chemical milli- and microreactors (Hartman and Jensen, 2009) in combination with the recent push of CFC e.g. for pharmaceutical synthesis (Siguemoto et al., 2020) or polymerization of macromolecules (Reis et al., 2019) renewed the interest in characterization of the flow behavior in such devices through the RTD (Boskovic and Loebbecke, 2008; Gobert et al., 2017; Hopley et al., 2019; Huber and Santiago, 2007; Vikhansky, 2011). For maximizing process intensification via flow chemistry, precise setting of residence time down to minutes and seconds is essential (Hessel, 2009). A broad residence time distribution generally might have a negative effect on conversions and/or selectivity in syntheses, and can lead to a wide size distribution in nanoparticle/cluster syntheses and polymer dispersity. In general, the RTD of the reactor should be as narrow as possible to ensure each fluid element has the same residence time. This requires the reduction of axial dispersion, which will not only yield higher efficiencies but also allow integration of the reactor unit with downstream processing (Hereijgers et al., 2015).

For realization of larger reaction times, a residence-time providing unit is required. Often a helically coiled capillary tube serves for this purpose. If centrifugal forces are sufficiently large, a secondary flow (Dean vortices) perpendicular to the primary axial flow is induced which contributes to a reduction in axial dispersion promoting plug flow (Janssen, 1976; Koutsky and Adler, 1964; Savage et al., 2024) and a narrowed RTD (Ruthven, 1971). Further narrowing of the RTD can be obtained by coiled tubes with flow inversion, where the direction of centrifugal forces is regularly reversed (Rossi et al., 2017; Saxena and Nigam, 1984; Schmalenberg et al., 2019). For other applications of the Taylor-Aris theory, such as the measurement of molecular diffusion coefficients (e.g. of large biomolecules (Sadriaj et al., 2022)) by injection of narrow sample plug into long coiled tubes, the influence of secondary flows on the band broadening should be insignificant. This can be ensured by operating below a transitional flow rate (Atwood and Goldstein, 1984).

With the increasing interest in flow chemistry (Guidi et al., 2020), appropriate modeling of the RTD comes into focus. Physically, the RTD is determined by the interplay between convective and diffusive transport. In the pure convection (PC) regime, molecular diffusion is negligible and each fluid element follows its streamline with no intermixing with neighboring elements. Then, the velocity profile causes fluid elements to spend different times within the reactor giving rise to a (usually unfavorable) wide RTD. In the PC limit, the RTDs of the solute and the solvent are identical and determined by the non-uniform velocity profile alone. Closed analytical forms of the diffusion-free RTD in laminar flows are known only for certain Newtonian, non-Newtonian or generalized velocity profiles (Emami Meibodi, 2022; Levenspiel, 2012; Osborne, 1975; Wörner, 2015) and few channel shapes (Erdogan and Wörner, 2013). Typical for the diffusion-free RTD of the PC regime are a sharp peak head corresponding to the maximum (centerline) velocity followed by long tails leading to infinite variance. The minimum residence time, which corresponds to the residence time of the fastest fluid elements, is commonly denoted as first-appearance time or breakthrough time. The other extreme is the pure diffusion regime which is without relevance for CFC. When convection and diffusion are both of importance, the RTD can – under certain conditions – be described by the axial dispersion (AD) model, either with the Taylor or the more general Taylor-Aris expression for dispersion. In this case, flow behavior shows minor deviations from ideal plug flow and the RTD is a close-to-symmetric bell shaped curve which can well be fitted by the AD model.

1.4. Dispersion regime map

Ananthakrishnan et al. (1965) developed a map showing a graphical summary of the regions with different dispersion regimes in a straight circular pipe as function of two non-dimensional parameters, the Peclet number $Pe = dU/D$ and the dimensionless time t/τ_d. Levenspiel (1999,

Fig. 15.2) adapted this diagram for selecting an appropriate RTD model by replacing the dimensionless time on the horizontal axis by $\lambda = L/d$, representing the ratio of length and inner diameter of the pipe. A further variant of this map for tracer dispersion in a capillary tube is given by Probstein (1994, Fig. 4.6.5). While the axes and regime boundaries differ, all these maps show the different regions in which the role of diffusion, dispersion, and convection vary in importance. In Fig. 1 (a) we show an adaptation of the Levenspiel map for the present paper. There are four main boundaries in Fig. 1(a), namely pure diffusion, pure convection, axial dispersion, and $\lambda_{\min}$. Axial dispersion is further subdivided into two regions where dispersion coefficients of Taylor and Taylor-Aris are appropriate, respectively. The remaining region of the dispersion regime map is denoted differently in literature. Ananthakrishnan et al. (1965, Fig. 8) indicated that in this region only numerical solution is applicable. Probstein (1994, Fig. 4.6.5) named that region as transition region, while Levenspiel (1999, Fig. 15.2) denoted the region which is shaded in gray in Fig. 1(a) as intermediate regime. Here we mainly use the terminology transition regime (TR), but consider it synonymous with intermediate regime. While Levenspiel did not specify the position of the diagonal lines enclosing the transition regime, the respective regime boundaries of Ananthakrishnan et al. (1965) are $0.012 \leq t/\tau_d \leq 0.8$. With $t \cong L/U$ the latter boundaries correspond to $1.25 \leq \alpha \leq 83.3$. The boundaries for the transition regime shown in Fig. 1(a) and used in this paper are $0.25 < \alpha < 125$, as explained below (Section 2.3).

Peclet numbers in microfluidics usually vary between 10 and 10^5 with molecular diffusivities ranging from 10^{-9} to 10^{-7} m^2/s (Stone et al., 2004), the lower value being typical for solute in water at room temperature. While the extension of the abscissa to $\lambda = 10^6$ in Fig. 1(a) is unrealistic for straight tubes, it is realistic for coiled tubes as for an inner diameter of 100 μm and a typical length of 10 m a value $\lambda = 10^5$ results. Accordingly, many CFC and microfluidic applications fall in the transition regime. For example, Gobert et al. (2017) characterized the RTD of various geometrically complex micro- and milliflow reactors in comparison to a wide range of classical tubular reactors (with inner diameter ranging from 0.4 to 4.8 mm). Most of the coiled tubular reactors made of flexible polymer tubes investigated are in the transition regime. Similarly, for flow-injection analysis, the most practical region is the transition regime where neither the pure convection model nor the axial dispersion model are applicable (Kolev, 1995; Vanderslice et al., 1981). Levenspiel (1999) suggests "If your system falls in the no-man's land between regimes, calculate the reactor behavior based on the two bounding regimes and then try averaging". Levenspiel gives, however, no advice how to perform this averaging in practice and the author is not aware of any paper on the subject how to properly average between the PC and AD regimes. Clearly, linear interpolation (Read, 1999) of the completely different RTDs is not suitable here. The interpolation method proposed by Bursal (1996) requires that the variance of the two PDFs is finite. Since the variance of the pure convection RTD is infinite, this method cannot be used here. The usual practice for characterization of milli- and microflow reactors falling in the transition regime, also adopted by Gobert et al. (2017), is therefore to model the measured RTD by one of the two classical flow models, the axial dispersion model and the pure convective flow model.

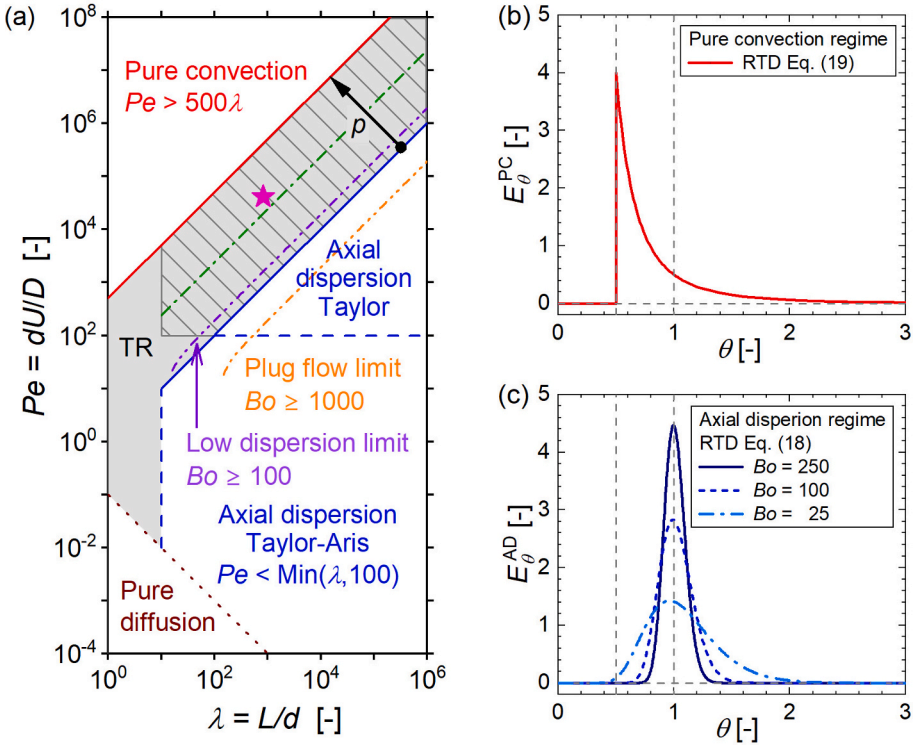

Fig. 1. (a) Regime map for dispersion in a straight tube adapted from Levenspiel (1999, Fig. 15.2). Straight lines in this log-log plot separate regions where different models apply. Diagonal upward solid red line: $Pe = 500\lambda$, diagonal upward solid blue line $Pe = \lambda$, horizontal dashed blue line $Pe = 100$, vertical dashed blue line $\lambda_{\min} = 10$, diagonal downward dotted brown line $Pe = 1/10\lambda$. In the grey-shaded transition regime (TR) neither the dispersion model nor the pure convection model are ideal. In this paper, a mechanistic model for the RTD in the hatched region is developed based on a regime transition parameter $0 < p < 1$ indicated by the black arrow. The diagonal upward dashed-dotted green line corresponding to $Pe=24\lambda$ represents the upper limit for the simplified compartment (dTiS) model. For a given Pe value, plug flow behavior results for λ values to the right of the plug flow limit (orange dash-dot-dot line, Eq. (17)). The magenta star symbol corresponds to experimental conditions related to the RTD of a coiled pipe (Gobert et al., 2017) to be discussed below (Section 4.2). (b) RTD of pure convection regime. (c) RTD of axial dispersion regime for different values of the Bodenstein number. For $Bo \geq 100$, dispersion is generally considered to be low. (For interpretation of the references to colour in this figure legend, the reader is referred to the web version of this article.)

1.5. Goal

The above discussion shows that there is a strong need in chemical engineering and other scientific and technical fields for a model that correctly describes dispersion in the transitional diffusion-convection regime and the associated RTD. However, to the best of the author's knowledge, a suitable mathematical model is still missing that can represent the transition from the skewed RTD of the PC regime (Fig. 1 (b)) to the almost symmetric bell-shaped RTD of the AD regime (Fig. 1 (c)) and satisfies the mathematical constraints of an RTD. The goal of the present paper is to develop a mathematical model which can describe this shape transition of the RTD and which is predictive in the sense that it depends on prior known parameters only.

To reach these goals, the transport of a passive tracer in a straight tube with circular cross section under fully developed laminar isothermal flow of an incompressible Newtonian fluid is studied theoretically. By assuming a radial concentration profile at the channel outlet which agrees with the concentration profiles of the pure convection and axial dispersion models in the respective limits, first an unclosed mechanistic model for the RTD in the transition regime with a single adjustable parameter is derived analytically from first physical principles. The mechanistic model is closed by fitting the free parameter to a case study of numerical RTD data from the literature, covering a very wide range of dispersion conditions (Dantas et al., 2014). The proposed mechanistic model is applicable in the hatched area of the dispersion regime map in Fig. 1(a). While the regime map is spanned by the normalized pipe length $\lambda = L/d$ and the Peclet number $Pe = dU/D$, the model depends on the sole dimensionless parameter $\alpha = a^2U/LD = Pe/4\lambda$, representing the ratio of the characteristic time scales of transversal transport by diffusion to longitudinal transport by advection. Since the mechanistic RTD model is mathematically rather complex, additionally a simpler model based on a compartment approach is derived which is, however, applicable only in a sub-region of the transition regime. It is expected that both models will be useful for predicting or characterizing dispersion behavior in flow chemistry and other flow systems where operating conditions fall in the transition regime.

2. Methodology

In the transition regime, diffusion can neither be neglected as is in the pure convection regime nor is diffusion sufficiently dominant to establish a uniform concentration distribution across the outlet plane as is the case for the axial dispersion regime. To exploit the full potential of CFC, mechanistic models for dispersion in the transient regime are required for design purposes. In this section, we present the theoretical basis for the development of our RTD models for the transition regime, which are described in Section 3.

2.1. Determining the RTD in experiment and simulation

The RTD is traditionally measured through a stimulus–response experiment by monitoring the change in concentration of a non-reactive tracer as it passes through the reactor. The term RTD is therefore usually implicitly associated with the solute. In this paper, we strictly distinguish between the RTD of the solute (tracer) and that of the solvent. The mean RT of solvent molecules which collectively create the Poiseuille flow is given by the space time. For various reasons, a solute molecule may move axially through the tube at a different average velocity (either greater or lesser) than the solvent (Brenner, 1990). In general, the mean RT of the solute equals that of the solvent only when the tracer is injected in flux by a temporal delta pulse and is detected in flux. The flow average or "mixing cup" concentration detected in flux is the concentration that would be measured if the liquid were collected at a certain axial distance (here at the outlet) and thoroughly mixed.

To determine the solute RTD theoretically or by numerical simulation, the injection of a passive tracer at the inlet and the detection of its mixing cup average concentration at the outlet must be mimicked. In the absence of reaction, the instantaneous solute concentration field is described by an advection–diffusion equation (Section 2.2.1). In combination with suitable initial conditions representing tracer injection (Section 2.2.2), analytical or numerical solutions of the solute advection–diffusion equation can be used to determine from the concentration distribution in the outlet plane the corresponding mixing cup concentration and the differential RTD (Section 2.2.3). Here, we are interested in the solute RTD for a pipe segment of length L, corresponding to a circular cylindrical reactor with volume $V_{\text{reactor}} = \pi a^2 L$, under Poiseuille flow of the solvent with constant solvent volumetric flow rate $Q = \pi a^2 U$. The length L is arbitrary and treated as a variable. It enters into the RTD models developed below only indirectly via dimensionless parameters, i.e., the Bodenstein number Bo and the normalized transversal diffusion time α.

2.2. Concentration field and RTD

2.2.1. Solute transport equation

We employ a cylindrical coordinate system with axial coordinate z and polar coordinates (r,φ), where the distance from the axis of the tube (r) is in the range $0 \le r \le a$. With the infinite pipe assumption, the axial coordinate is in the range $-\infty < z < \infty$. The formal entrance and outlet planes of the tracer are located at $z = 0$ and $z = L$, respectively. We assume that the distribution of solute is rotationally symmetrical around the z axis and denote its molar concentration at time t by $c(r, z, t)$. Concerning hydrodynamics of the solvent, we assume a fully developed unidirectional steady and axisymmetric laminar flow of an incompressible viscous Newtonian fluid (kinematic viscosity ν). We further assume Reynolds numbers $Re = dU/\nu < 2000$ so that the velocity profile is parabolic (Poiseuille flow). Entrance effects on the RTD, as discussed in Ham et al. (2011), are neglected here.

With the latter assumptions, the mass balance for a conserved single-component solute in a volume element of the tube yields the microscale advection–diffusion equation

$$\frac{\partial c}{\partial t} + \underbrace{2U\left(1 - \frac{r^2}{a^2}\right)}_{=u(r)}\frac{\partial c}{\partial z} = D\left[\frac{1}{r}\frac{\partial}{\partial r}\left(r\frac{\partial c}{\partial r}\right) + \frac{\partial^2 c}{\partial z^2}\right], \tag{1}$$

which describes the transport and temporal evolution of solute concentration. To transfer Eq. (1) in an appropriate non-dimensional form, we define $C = c/c_{\text{ref}}$ with reference molar concentration $c_{\text{ref}} = m/V_{\text{reactor}}$. Here, m denotes the amount of tracer moles injected during the pulse input. For normalization of coordinates and time different options exist. Following Kolev and van der Linden (1991), we normalize the radial and axial coordinates differently and define $R = r/a$ and $Z = z/L$ so that $0 \le R \le 1$ and $-\infty \le Z \le \infty$, respectively. Since we include in our analysis the case of pure convection ($D = 0$), a normalization of time by the time scale of transverse diffusion $\tau_{\text{d}} = a^2/D$ is not meaningful. Instead, we normalize time by the space time $\tau_{\text{s}} = L/U$ and introduce the reduced time $\theta = t/\tau_{\text{s}} = tU/L$. Then the non-dimensional equation for the transport of a solute in cylindrical coordinates is

$$\frac{\partial C}{\partial \theta} + \underbrace{2\left(1 - R^2\right)}_{=V(R)}\frac{\partial C}{\partial Z} = \frac{4\lambda}{Pe}\left[\frac{1}{R}\frac{\partial}{\partial R}\left(R\frac{\partial C}{\partial R}\right) + \frac{1}{4\lambda^2}\frac{\partial^2 C}{\partial Z^2}\right], \tag{2}$$

where $V = u(r)/U = 2\left(1 - R^2\right)$ denotes the normalized Poiseuille velocity profile.

The latter two partial differential equations are linear in concentration and can be solved by Laplace transformation for given initial and boundary conditions. However, inverting the solution back often results in infinite series with low rate of convergence for large values of the

Peclet number (Martin, 2000). Gill and Sankarasubramanian (1970) solved Eq. (1) analytically using the series expansion method originally proposed by Gill (1967) by treating the axial dispersion coefficient as a function of time. For references to analytical solutions of Eq. (1) by other mathematical methods, such as long-time asymptotic expansion technique, two-scale perturbation approximation and Lyapunov-Schmidt technique the interested reader is referred to Jiang and Chen (2018) and Guan and Chen (2024). In general, the advection–diffusion equation for laminar flow through a cylindrical tube is solved numerically (Ananthakrishnan et al., 1965; Bailey and Gogarty, 1962; Bate et al., 1973; Bate et al., 1969; Ekambara and Joshi, 2004; Farrell and Leonard, 1963; Yu, 1976). In the transition regime, adjustment of any one, or all, of the parameters U, a and D can fundamentally alter the shape of the dispersion curve resulting from bolus injection (Bate et al., 1973). Numerical solutions covering a wide range of the Peclet number $1 \le Pe \le 10^5$ and dimensionless time $10^{-8} \le tD/a^2 \le 10^2$ are consistent with all previously reported special cases (Ekambara and Joshi, 2004).

Except for extremely slow flows and at extremely short length scales, longitudinal molecular diffusion is vastly dominated by advection. If one follows Taylor (1953) and neglects axial diffusion, then Eq. (2) depends on the parameter $\lambda/Pe = LD/d^2U$ only. Steffani and Platzer (2002) identified the inverse ratio d^2U/LD as modified Peclet number ($\overline{Pe}^*$ in their nomenclature) and noted that "the parameter $\overline{Pe}^*$ alone is apt to characterize unambiguously cases of laminar (tube) flow, which is in part a confirmation of earlier works, but has yet not found to be stated in this clearness". Other researchers interpreted the non-dimensional group $LD/(d^2U)$ as a Fourier number based on the space time and either the diameter (Golbig et al., 2005) ($Fo_\mathrm{d} = \tau_\mathrm{s}D/d^2$) or radius (Nagy et al., 2012) ($Fo_a = \tau_\mathrm{s}D/a^2$) of the tube. Here, we follow Wissler (1969) and interpret $\alpha = \tau_\mathrm{d}/\tau_\mathrm{s} = a^2U/LD = Pe/4\lambda = 1/Fo_a$ as ratio between the time scales of transversal diffusion and longitudinal advection (space time). The results of the present paper confirm and reinforce the statement of Steffani and Platzer (2002) concerning the outstanding importance of parameter d^2U/LD, respectively — in present notation — the normalized transversal diffusion time $\alpha = a^2U/LD$.

2.2.2. Initial conditions representing tracer injection

Experimental measurement of the RTD is commonly conducted by tracer response techniques. Usually, the inert tracer substance is injected into the continuous solvent stream at the inlet plane either in the form of an instantaneous pulse (mathematically described as Dirac delta function), a step (Heaviside function) or a rectangular pulse (bolus). A pulse input of tracer requires injection of a quantity of tracer within a period of time much shorter than the average residence time in the reactor; on the other hand, a step input requires a stable and constant source of tracer (Huang and Seinfeld, 2019). For the pulse input method, the tail of the RTD will be strongly affected by noise whereas for the step input method the tracer may affect fluid properties of the solvent. At the outlet plane, the transient concentration or a proportional signal is measured and processed to determine the RTD. The stimulus–response principle can be imitated by solving Eq. (2) with appropriate initial and boundary conditions. The injections are considered to occur at zero time ($\theta = 0$) at axial position $Z = 0$ while the measurement plane is located at $Z = 1$. In this paper, only flux pulse injections in form of a delta function are considered. The step response is then simply the time integral of the pulse response.

Mathematically, one can distinguish between delta functions, which represent pulse injections in time or in space. For the axial dispersion model, only flux delta injection in time and mixing cup measurement at the outlet gives a solute RTD with first moment equal to the mean residence time of the solvent (Kreft and Zuber, 1978). Flux delta injection in time can hardly be realized experimentally, since it requires a finite amount of tracer be injected in zero time (Himmelblau and Bischoff, 1968, pg. 116). In the present study, we consider delta injection in space. The reason is that the application of a similar procedure as presented below for a spatial pulse (Section 3) does not allow the analytical calculation of all integrals when a temporal pulse is used. An ideal flux pulse injection in space indicated by symbol $\uparrow z$ can be represented by the initial condition

$$c_{\uparrow z}(r,z)|_{t=0} = \frac{m}{A}\frac{u(r)}{U}\delta(z) \tag{3}$$

The multiplication by the velocity profile $u(r)$ implies that the tracer with total injected molar amount m is added in quantities proportional to the flow through each point in the injection plane (flux injection).

2.2.3. Analytical calculation of the RTD from the concentration distribution in the outlet plane

The residence time distribution can be quantitatively described by the time that individual fluid elements spend in the reactor. For the pulse tracer method, the differential RTD can be defined as

$$E(t) = \frac{c_\mathrm{cup}(t)}{\int_0^\infty c_\mathrm{cup}(t)\mathrm{d}t} = \frac{C_\mathrm{cup}(t)}{\int_0^\infty C_\mathrm{cup}(t)\mathrm{d}t}, \tag{4}$$

where $c_\mathrm{cup}(t)$ is the mixing cup tracer concentration at the outlet plane as a function of time and $C_\mathrm{cup} = c_\mathrm{cup}/c_\mathrm{ref}$. By definition it is $\int_0^\infty E(t)\mathrm{d}t = 1$ independent of the amount of the injected tracer.

The normalized mixing cup average concentration C_cup in Eq. (4) can be calculated from the concentration field in the outlet plane $C_\mathrm{out}(r,t) = C(r, z = L, t)$ by a flow-rate weighted area average as

$$C_\mathrm{cup}(\theta) = \frac{1}{\pi a^2 U}\int_0^a C_\mathrm{out}(r,t)\cdot u(r)\cdot 2\pi r\cdot \mathrm{d}r = \frac{1}{2}\int_0^2 C_\mathrm{out}(\theta|V)\cdot V\cdot \mathrm{d}V, \tag{5}$$

where the last expression follows from the substitution $V = u(r)/U = 2\left(1 - r^2/a^2\right)$. The moments of the mixing cup concentration about the origin can be written as

$$\mu_n = \int_0^\infty \theta^n\cdot C_\mathrm{cup}(\theta)\cdot \mathrm{d}\theta = \frac{1}{2}\int_0^2 \left\{\int_0^\infty \theta^n\cdot C_\mathrm{out}(\theta|V)\cdot \mathrm{d}\theta\right\}\cdot V\cdot \mathrm{d}V, \tag{6}$$

where n is a non-negative integer and the normalized velocity profile V has become a dummy variable of integration. For a given outlet concentration $C_\mathrm{out}(\theta|V)$, the integrals in Eqs. (5) and (6) are always carried out analytically in the present paper using support by Mathematica software. For some cases, when Mathematica was unable to calculate the single integral over θ in Eq. (6) analytically, the order of integration was reversed, resulting in the double integral in Eq. (6). Carrying out analytically the integration of the inner integral in the curvy brackets first, the outer integral could always be calculated analytically as well.

Multiplying Eq. (4) by the space time yields the non-dimensional RTD

$$E_\theta(\theta) = \tau_\mathrm{s}\cdot E(t) = \frac{C_\mathrm{cup}(\theta)}{\mu_0}, \tag{7}$$

which fulfills the normalization condition $\int_0^\infty E_\theta \mathrm{d}\theta = 1$. For the normalized mean value ($\overline{\theta}$) and variance (σ_θ^2) we obtain the relations

$$\overline{\theta} = \frac{\bar{t}_\mathrm{E}}{\tau_\mathrm{s}} = \int_0^\infty \theta E_\theta(\theta)\mathrm{d}\theta = \frac{\mu_1}{\mu_0}, \tag{8}$$

$$\sigma_\theta^2 = \frac{\sigma_\mathrm{E}^2}{\tau_\mathrm{s}^2} = \int_0^\infty (\theta - \overline{\theta})^2 E_\theta(\theta)\,\mathrm{d}\theta = \int_0^\infty \theta^2 E_\theta(\theta)\,\mathrm{d}\theta - \overline{\theta}^2 = \frac{\mu_2}{\mu_0} - \frac{\mu_1^2}{\mu_0^2} \tag{9}$$

Eq. (8) yields 1 only when the mean residence time $\bar{t}_\mathrm{E}$ determined from the tracer response technique equals the space time τ_s. In this case it is

$$\overline{\theta} = \int_0^\infty \theta E_\theta(\theta)\mathrm{d}\theta = 1, \quad \sigma_\theta^2 = \int_0^\infty (\theta - 1)^2 E_\theta(\theta)\mathrm{d}\theta \tag{10}$$

We remark, that in experimental RTD studies using tracer technology, time is – in contrast to the present paper – sometimes not normalized by the space time but by the measured mean residence time $\bar{t}_E$ of the solute. Such normalization results in different definitions for reduced time, reduced mean RT and reduced variance as used here.

2.3. Limiting cases

Taylor (1953) has presented solutions of Eq. (1) for two limiting cases: an early (pre-asymptotic) period where dispersion is determined by advection alone and a late asymptotic period. At short times $t < a^2/D = \tau_d$ corresponding to $\theta < \alpha$, dispersion is convection dominated leading to a rapid increase in axial length of the solute band and significant cross-stream diffusion. For asymptotically long times $t \gg a^2/D$ corresponding to $\theta \gg \alpha$, a quasi-equilibrium is reached where the longitudinal stretching by axial convection is balanced by radial diffusion. The resulting cross-stream averaged axial concentration profile is Gaussian, resembling that of diffusive transport alone with an increased diffusion coefficient, and travels in a plug-like fashion at the average flow velocity. The Taylor-Aris dispersion relation is true asymptotically only after the tracer has sampled each streamline with equal opportunities through the whole cross-section (Guan and Chen, 2024). Below we discuss both limiting regimes of the concentration field and the related RTD, starting with the long time axial-dispersed plug flow regime followed by the early-time convection dominated regime. Graphical illustrations of the concentration fields at early and late times are provided in the Supplemental Material (Fig. S.1).

2.3.1. Asymptotic axial dispersion regime and limit α_{AD}

For long times $t \gg a^2/D$, the cross-sectional average of the unsteady three-dimensional concentration field within a tube evolves as a one-dimensional convective diffusion equation (Taylor, 1953). In this regime, the axial dispersion model is valid having its origins in the cross-sectional averaged advection–diffusion equation developed in the pioneering work of Taylor (1953, 1954) and the longitudinal concentration moment analysis of Aris (1956). We use the hat symbol to denote variables related to the transverse area average over the cross-section defined by

$$\widehat{(\cdot)} = \frac{2}{a^2}\int_0^a (\cdot) r \mathrm{d}r \tag{11}$$

With the prime denoting the deviation, the concentration field can be split into its cross-sectional average and r-dependent part as $c(r,z,t) = \widehat{c}(z,t) + c'(r,z,t)$, where $\widehat{c'} = 0$. By inserting this decomposition into Eq. (2), averaging over the channel cross section and introducing some simplifying assumptions (Sharp, 1993), the following one-dimensional Fokker-Planck type advection–diffusion equation for the mean (cross-average) concentration can be derived

$$\frac{\partial \widehat{c}}{\partial t} + U\frac{\partial \widehat{c}}{\partial z} = D_{ax}\frac{\partial^2 \widehat{c}}{\partial z^2} \tag{12}$$

In Eq. (12), D_{ax} is the effective axial Taylor-Aris dispersion coefficient (Aris, 1956; Taylor, 1953), which is the sum of the molecular diffusion coefficient (D) and the shear dispersion due to external flow

$$D_{ax} = D + \frac{a^2U^2}{48D} \tag{13}$$

It should be noted that Eq. (13) predicts $D_{ax} \to \infty$ as $D \to 0$, but in this limit the assumption of small lateral concentration gradients breaks down and the result is no longer valid (Sharp, 1993). For $D \ll a^2U^2/48D$ axial molecular diffusion may be neglected (Taylor, 1954). In this case, the longitudinal dispersion coefficient in Eq. (13) reduces to the Taylor dispersion coefficient $a^2U^2/48D$ which is inversely proportional to the molecular diffusion coefficient of the solute. Numerical results of Ananthakrishnan et al. (1965) indicate that neglecting D in Eq. (13) against the Taylor dispersion coefficient is applicable provided $Pe \geq 100$. Following Levenspiel (1999, Fig. 15.2), we adopted this limit in Fig. 1(a) (horizontal dashed blue line).

Among the different variants of dispersion models, the partial differential Eq. (12) is known as the axially dispersed plug flow model (Kolev, 1995). Since the pre-factor $u(r)$ of the convective term in Eq. (1), representing the parabolic radial velocity profile, is in Eq. (12) replaced by the constant plug flow velocity U, the radial variable is eliminated completely and an ideal plug flow is superimposed by axial dispersion while the degree of backmixing during flow is uniquely characterized by D_{ax}. The solution of Eq. (12) depends on the initial conditions and on the boundary conditions at the inlet and outlet of the control domain (Brenner, 1962; Colli and Bisang, 2015; Kreft and Zuber, 1978; Trinidad et al., 2006). For closed-to-diffusion boundary conditions, no analytical solutions exist but Eq. (12) can be resolved by the use of Laplace transforms. For the pulse initial condition, the solution depends on whether the delta function is formulated in space or time. Both initial conditions of the AD model have different physical meanings, which result in different analytical solutions (Hsu and Dranoff, 1986).

The solution of Eq. (12) subject to the macroscale initial condition $\widehat{c}(z, t=0) = m{\cdot}\delta(z)/A$ representing a spatial delta pulse in the longitudinal direction is (Levenspiel and Smith, 1957)

$$\widehat{c}^{\,AD}_{\uparrow z}(z,t) = \frac{m}{A}\frac{1}{\sqrt{4\pi D_{ax}t}}{\cdot}\exp\left[-\frac{(z-U{\cdot}t)^2}{4D_{ax}t}\right] \tag{14}$$

The non-dimensional form of Eq. (14) becomes

$$\widehat{C}^{\,AD}_{\uparrow z}(\theta, Z|Bo) = \sqrt{\frac{Bo}{4\pi\theta}}{\cdot}\exp\left[-\frac{Bo}{4}\frac{(Z-\theta)^2}{\theta}\right] \tag{15}$$

The characteristic dimensionless number in Eq. (15) is the Bodenstein number

$$Bo = \frac{LU}{D_{ax}} = \frac{\lambda Pe}{1 + Pe^2/192} = \frac{1}{4\alpha}\frac{Pe^2}{1 + Pe^2/192}, \tag{16}$$

which represents the time scale ratio between longitudinal dispersion (L^2/D_{ax}) and longitudinal advection (L/U). It can also be interpreted as a Peclet number based on the pipe length and the axial dispersion coefficient (Bremer and Turek, 2024). The inverse D_{ax}/LU is sometime denoted as vessel dispersion number (Levenspiel, 1999). Higher Bo numbers indicate reduced axial mixing, while lower Bo numbers indicate higher mixing degrees. The limit $Bo \to 0$ corresponds to full backmixing, which is the ideal state to be reached in a continuous stirred tank reactor (CSTR). In this case, each portion of the material has the same chance to be discharged at the outlet, regardless how long it has already been inside the CSTR. For $Bo > 100$ axial dispersion is considered low. Ideal plug flow with no backmixing is theoretically obtained in the limit $Bo \to \infty$. Taking $Bo = 1000$ as practical value instead (Nagy et al., 2012), the plug flow limit following from Eq. (16) as displayed in Fig. 1(a) is

$$\lambda_{PF} \geq \frac{1000}{Pe}\left(1 + \frac{Pe^2}{192}\right) \tag{17}$$

For $Pe \geq 100$ as considered here (hatched region in Fig. 1(a)) it is $Pe^2/192 \geq 52.08 \gg 1$ so that the Bodenstein number can be approximated as $Bo \approx 48/\alpha$.

If one sets in Eq. (15) $Z = 1$ and calculates the integrals in Eqs. (5)–(7) for this outlet concentration, one obtains with $\mu_0^{AD\uparrow z} = 1$ the non-dimensional differential RTD

$$E_\theta^{AD\uparrow z}(\theta|Bo) = C_{cup}^{AD\uparrow z}(\theta) = \sqrt{\frac{Bo}{4\pi\theta}}\exp\left[-\frac{Bo}{4}\frac{(1-\theta)^2}{\theta}\right], \tag{18}$$

first derived by Levenspiel and Smith (1957) and shown in Fig. 1(c). Notably, the non-dimensional differential RTD and the normalized

outlet mixing cup concentration are identical for this case. The reduced mean and reduced variance of this RTD are $\overline{\theta}_{\mathrm{AD}\uparrow z} = 1 + 2/Bo$ and $\sigma^2_{\theta,\mathrm{AD}\uparrow z} = 2/Bo + 8/Bo^2$, respectively. To fit an experimental RTD of a reactor by the AD model, Bo is therefore often determined from the measured variance of the RTD, which is as the second central moment a measure for the degree of dispersion around the mean.

We remark, that the solution $\widehat{c}_{\uparrow t}(z,t)$ of Eq. (12) subject to the condition $\widehat{c}(z=0,t) = m{\cdot}\delta(t)/Q$ representing a delta pulse in time is related to Eq. (14) by $\widehat{c}_{\uparrow t}(z,t) = z\widehat{c}_{\uparrow z}/tU$ (Hsu and Dranoff, 1986; Hubert, 1970; Kreft and Zuber, 1979). Similarly, the corresponding RTDs are related by $E_\theta^{\mathrm{AD}\uparrow t} = E_\theta^{\mathrm{AD}\uparrow z}/\theta$. With first and second moments about the origin equal to unity, $E_\theta^{\mathrm{AD}\uparrow t}$ agrees with the non-dimensional differential RTD derived by Gibilaro (1978), where the mean RT of the solute agrees with the mean RT of the solvent. The reduced variance of this RTD is $\sigma^2_{\theta,\mathrm{AD}\uparrow t} = 2/Bo$.

The axial dispersion model can be used to model laminar flow if the reactor is sufficiently long so that radial diffusion effectively removes radial concentration gradients. For measuring the molecular diffusion coefficient by dispersion theory in a circular tube, Taylor (1954) suggested the criterion $L \gg a^2U/4D$ corresponding to $\alpha \ll 4$. Synonymously, the validity of the AD model requires that the time scale of transversal diffusion τ_d is very low compared to the time scale of longitudinal convection τ_s. The boundary for the axial dispersion region can thus be written as $\alpha = \tau_\mathrm{d}/\tau_\mathrm{s} = Pe/4\lambda \leq \alpha_\mathrm{AD}$ where α_AD is a constant. If a 10:1 ratio is permitted between the terms of the inequality $\tau_\mathrm{d} \ll \tau_\mathrm{s}$, one obtains $\alpha_\mathrm{AD} = 0.1$ corresponding to $Pe \leq 0.4\lambda$; this value is used in the book of Probstein (1994, Fig. 4.6.5) (note that there the Peclet number is based on the pipe radius instead on the diameter as here). A much larger value of $\alpha_\mathrm{AD} \approx 1$ corresponding to $Pe \leq 4\lambda$ is used in the book of Levenspiel (1999, Fig. 15.2). In this work we apply a criterion that lies between the two latter values and use $\alpha_\mathrm{AD} = 0.25$ corresponding to $Pe \leq \lambda$.

2.3.2. Pure convection regime and limit α_{PC}

The short time convective dispersion regime ($\theta < \alpha$) is also known as kinematic or "ballistic" dispersion regime (Ajdari et al., 2006; Huber and Santiago, 2008). In this regime time is too short, or interpreted differently, the pipe is not long enough to achieve radial uniformity of the solute at the outlet. The influence of the velocity profile is thus very important. In the limit of complete absence of molecular diffusion ($D = 0$), this regime remains, so to speak, forever and is known as pure convection regime. For the pure convection regime, the right-hand sides of Eq. (1) and Eq. (2) vanish and the solute RTD is determined exclusively by the velocity field of the solvent. The RTD of the PC regime for the parabolic velocity profile of pressure driven Poiseuille tube flow is (Bosworth, 1948)

$$E_\theta^\mathrm{PC} = H(\theta - \theta_\mathrm{f}){\cdot}\frac{\theta_\mathrm{f}}{\theta^3} \tag{19}$$

Here, $\theta_\mathrm{f} = U/U_\mathrm{max} = 0.5$ denotes the normalized first-appearance time of Poiseuille flow and H the Heaviside function, $H(\theta - \theta_\mathrm{f}) = 1$ if $\theta \geq \theta_\mathrm{f}$ and $H(\theta - \theta_\mathrm{f}) = 0$ otherwise. The mean value of the pure convection RTD in Eq. (19) is 1 and the variance is infinite. An illustration of the RTD $E_\theta^\mathrm{PC}(\theta)$ in the pure convection regime is shown in Fig. 1(b).

The pure convection model is valid when the diffusion term on the right side of Eq. (2) is small as compared to the convection term on the left side (Probstein, 1994). The criterion to neglect radial diffusion may be written as $Pe \gg \lambda$ while that for neglecting longitudinal diffusion is $Pe \gg 1/\lambda$. Here we assume $\lambda \geq \lambda_\mathrm{min} = 10$ so that for $Pe \gg \lambda$ the condition $Pe \gg 1/\lambda$ is automatically satisfied. The boundary in Fig. 1(a) for the validity of the PC model can thus be written as $\alpha = \tau_\mathrm{d}/\tau_\mathrm{s} = Pe/4\lambda \geq \alpha_\mathrm{PC}$, where α_PC is a constant. If a 10:1 ratio is permitted between the terms of the inequality $\tau_\mathrm{d} \gg \tau_\mathrm{s}$, this yields $\alpha_\mathrm{PC} = 10$ corresponding to $Pe \geq 40\lambda$. A value corresponding to $\alpha_\mathrm{PC} = 10$ is used in the regime map of Probstein (1994, Fig. 4.6.5). In this paper, we permit for the validity of the pure convection regime a 125:1 ratio so that $\alpha_\mathrm{PC} = 125$ corresponding to $Pe \geq 500\lambda$, which also represents the border between the PC and transition regime in the regime map of Levenspiel (1999, Fig. 15.2).

3. Model development

In this section we present two novel models for the RTD in the transition regime, a mechanistic first principle one derived from the governing equation for solute transport and a descriptive one based on a compartment approach. Both models are first developed with one free adjustable parameter. To close the models and make them predictive, the free parameter of each model is then related to the normalized transversal diffusion time α.

3.1. Mechanistic transition regime model (MTR model)

The starting point for the development of the mechanistic model is the dimensional advection–diffusion equation describing solute transport under Poiseuille flow of the solvent, Eq. (1). The normalized version of this partial differential equation given by Eq. (2) shows that solutions depend on the two parameters Pe and λ spanning the dispersion regime map (Fig. 1 a). In Section 2.2.3 we have demonstrated how solutions of Eq. (2) under fundamental initial conditions and appropriate boundary conditions can be used to calculate the RTD from the time dependent concentration field in the outlet plane. If the time-dependent concentration distribution in the outlet plane would be known for the transition regime, the RTD could thus be computed. However, there exists no analytical solution of Eq. (2) valid in the transition regime that would allow for analytical calculation of the integrals in Eq. (5) and Eq. (6). The present strategy outlined below is therefore to assume a heuristic approximation of this outlet concentration field instead.

3.1.1. Strategy of model development

Following Taylor (1953) and neglecting longitudinal molecular diffusion simplifies the normalized solute transport equation, Eq. (2), to the form

$$\frac{\partial C}{\partial \theta} + 2\left(1 - R^2\right)\frac{\partial C}{\partial Z} = \frac{1}{\alpha}\frac{1}{R}\frac{\partial}{\partial R}\left(R\frac{\partial C}{\partial R}\right) \tag{20}$$

Commonly used boundary conditions in radial direction are $\partial C/\partial R = 0$ at both, $R = 0$ (symmetry axis) and $R = 1$ (the tube wall is impenetrable to solute). Boundary conditions in axial direction are classified as "open" if tracer transport across the boundary is allowed and are denoted as "closed" otherwise. Here we assume that the pipe extends to infinity in both axial directions and employ the far-field axial boundary conditions $C \to 0$ as $|Z| \to \infty$. These correspond to co-called "open-open" boundaries enabling tracer flux through the inlet ($Z = 0$) and outlet ($Z = 1$) planes of the control domain. Solutions of Eq. (20) depend only on the single parameter $\alpha = Pe/4\lambda$.

If we perform cross-sectional averaging on Eq. (20) and apply Taylor's assumptions, we obtain

$$\frac{\partial \widehat{C}}{\partial \theta} + \frac{\partial \widehat{C}}{\partial Z} = \frac{\alpha}{48}\frac{\partial^2 \widehat{C}}{\partial Z^2} \tag{21}$$

The solution of Eq. (21) for an initial delta pulse in space is

$$\widehat{C}^\mathrm{AD}_{\uparrow z}(\theta, Z|\alpha) = \sqrt{\frac{12}{\pi\alpha\theta}}{\cdot}\exp\left[-\frac{12}{\alpha}\frac{(Z-\theta)^2}{\theta}\right] \tag{22}$$

The corresponding RTD is

$$E^\mathrm{AD}_\theta(\theta|\alpha) = C^\mathrm{AD}_\mathrm{out}(\theta|\alpha) = \widehat{C}^\mathrm{AD}_{\uparrow z}(\theta, Z|\alpha) = \sqrt{\frac{12}{\pi\alpha\theta}}{\cdot}\exp\left[-\frac{12}{\alpha}\frac{(1-\theta)^2}{\theta}\right] \tag{23}$$

The non-dimensional mean and variance are $\overline{\theta}_\mathrm{AD} = 1 + \alpha/24$ and $\sigma^2_{\theta,\mathrm{AD}} =$

$\alpha/24 + \alpha^2/288$, respectively. For small extends of dispersion (i.e., if $D_{ax}/LU = 1/Bo \approx \alpha/48$ is below 0.01) the spreading tracer curve does not significantly change in shape as it passes the measuring point during the time it is being measured (Levenspiel, 1999). Under these conditions the solution of Eq. (21) gives the symmetrical (AD→ADS) curves

$$E_\theta^{\mathrm{ADS}}(\theta|\alpha) = \widehat{C}_{\mathrm{ADS}}(\theta, Z=1|\alpha) = \sqrt{\frac{12}{\pi\alpha}}\cdot\exp\left[-\frac{12}{\alpha}(1-\theta)^2\right] \tag{24}$$

The non-dimensional mean RT is unity and the RTD in Eq. (24) corresponds to a normal (Gaussian) distribution with standard deviation $\sqrt{\alpha/24}$ and amplitude $\sqrt{12/\pi\alpha}$.

The present strategy for determining a mechanistic model for the RTD in the transition regime is to replace the unknown transient concentration distribution in the outlet plane fulfilling Eq. (20) by a heuristic approximation. This postulated outlet concentration $C_{\mathrm{out}}^{\mathrm{MTR}}(\theta, R, Z=1|\alpha)$ is utilized to compute E_θ^{MTR} by evaluating the integrals in Section 2.2.3 while keeping the entire procedure analytical. In order to be physically meaningful, the postulated outlet concentration should obey features of the axial dispersion regime and the pure convection regime while the RTD of the transition regime reduces to both cases in the limits. For the AD regime with spatial delta pulse as initial condition, the RTD equals the radially uniform outlet concentration and is given by Eq. (23). The RTD of the PC regime for pressure driven Poiseuille tube flow is given by Eq. (19). This RTD is a scale-invariant power law distribution (Pareto distribution).

3.1.2. Scale-variant approximation of pure convection RTD

The present procedure for developing a model for the RTD in the transition regime requires a scale-variant approximation of Eq. (19). To that end we consider the effects of a small amount of diffusion on the pure convection RTD. Bosworth (1948) presented a theoretical analysis of the effects of small amounts of radial and of small amounts of longitudinal diffusion on the RTD in laminar pipe flow and noted two modifications as compared to Eq. (19), where diffusion is absent. In the first place, the sharp cut-off at the head of the RTD is replaced by one which is more gradual the lower the value of $\sqrt{\lambda Pe/2} = \lambda\sqrt{2\alpha}$. This is because of diffusion some molecules have a residence time less than θ_f. In the second place, the operation of diffusion replaces the inverse cube law distribution curve in Eq. (19) by one in which values at high residence times are somewhat larger. This flattening of the distribution curve at high values of θ is the more pronounced the lower the value of $\sqrt{\alpha}$.

In the present paper, we take into account the effect of a small amount of diffusion by considering the advection equation

$$\frac{\partial c}{\partial t} + u(r)\frac{\partial c}{\partial z} = 0 \tag{25}$$

in combination with a modification of the initial condition. To allow for a fully analytical treatment, we replace the spatial delta function $\delta(z)$ in Eq. (3) by a regularized version. There exists several options for doing so. To establish the required connection with the concentration field in Eq. (14) resulting in the AD model, we choose the exponential relationship

$$\delta_{z,\varepsilon}(z|\varepsilon) = \frac{1}{\varepsilon\sqrt{\pi}}\exp\left(-\frac{z^2}{\varepsilon^2}\right) \tag{26}$$

Here, ε is a small positive parameter with the dimension of a length scale which will be related to the diffusion coefficient. The initial condition in Eq. (3) then becomes

$$c_{\uparrow z,\varepsilon}(r,z)\big|_{t=0} = \frac{m}{A}\frac{u(r)}{U}\frac{1}{\varepsilon\sqrt{\pi}}\exp\left(-\frac{z^2}{\varepsilon^2}\right) \tag{27}$$

We choose the length scale as $\varepsilon = 4\lambda^2 D/U$ where we assume $0 < D \ll a^2U/L$ corresponding to $\alpha \gg 1$. With $L/\varepsilon = \alpha$, Eq. (27) can be expressed as

$$\left.\frac{c_{\uparrow z,\varepsilon}(r,z)}{c_{\mathrm{ref}}}\right|_{t=0} = C_{\uparrow z,\varepsilon}(V,Z)\big|_{\theta=0} = \frac{\alpha}{\sqrt{\pi}}\cdot V(R)\cdot\exp\left(-\alpha^2 Z^2\right) \tag{28}$$

The solution of Eq. (25) subject to the axial boundary conditions $C = 0$ at $Z = \pm\infty$ and the initial condition in Eq. (28) is

$$\begin{aligned} C_{\mathrm{CDP}}(R,Z,\theta|\alpha) &= \frac{\alpha}{\sqrt{\pi}}\cdot 2\left(1-R^2\right)\cdot\exp\left[-\alpha^2\left(Z-2\theta\left(1-R^2\right)\right)^2\right] \\ &= \frac{\alpha}{\sqrt{\pi}}\cdot V\cdot\exp\left[-\alpha^2(Z-V\theta)^2\right], \end{aligned} \tag{29}$$

where the acronym CDP stands for "convection dominated preliminary". Inserting Eq. (29) with $Z = 1$ into Eq. (6) yields for the zero moment about the origin the result

$$\begin{aligned} \mu_0^{\mathrm{CDP}} &= \frac{1}{2}\int_0^2\left\{\int_0^\infty \frac{\alpha}{\sqrt{\pi}}\cdot V\cdot\exp\left[-\alpha^2(1-V\theta)^2\right]\cdot\mathrm{d}\theta\right\}\cdot V\cdot\mathrm{d}V \\ &= \frac{1}{2}[1+\mathrm{erf}\ (\alpha)] \end{aligned} \tag{30}$$

In the limit $\alpha\to\infty$ corresponding to $D = 0$ it is $\mu_0^{\mathrm{CDP}} = 1$. For finite values of α corresponding to $D > 0$ it is $\mathrm{erf}(\alpha) < 1$ and Eq. (30) yields $\mu_0^{\mathrm{CDP}} < 1$. The concentration field in Eq. (29) does thus not assure that the entire injected tracer amount has traversed through the outlet plane at infinite time. For the case $D > 0$, the advection equation of Eq. (25) should be replaced by the advection–diffusion equation of Eq. (1) which requires a boundary condition for $\partial c/\partial r$ at $r = a$. To ensure that the entire injected tracer amount leaves the outlet plane, a no-penetration boundary condition at the wall corresponding to $(\partial C/\partial R)|_{R=1} = 0$ is appropriate. For the concentration field in Eq. (29) it is $(\partial C_{\mathrm{CDP}}/\partial R)|_{R=1} < 0$ for finite α. This corresponds for $\alpha < \infty$ to a permeable wall so that not all tracer amount injected at the inlet reaches the outlet plane. It should be noted that the concentration profile in Eq. (29) is for $\alpha < \infty$ no solution of the advection–diffusion equation of Eq. (20) in combination with the no-penetration boundary condition at the tube wall.

The mean value of the outlet concentration distribution in Eq. (29) less than 1 for finite α is undesirable. To increase the mean value, we need to add skewness in the sense that the relative contribution to the distribution is decreased for $\theta < 1$ while it is increased for $\theta > 1$. For this purpose, we heuristically replace α in Eq. (29) by $\alpha/\sqrt{\theta}$ to obtain the convection dominated (CD) concentration field as

$$C_{\uparrow z}^{\mathrm{CD}}(V,Z,\theta|\alpha) = \frac{\alpha}{\sqrt{\pi\theta}}\cdot V\cdot\exp\left[-\alpha^2\frac{(Z-V\theta)^2}{\theta}\right] \tag{31}$$

Inserting Eq. (31) with $Z = 1$ into Eq. (6) and calculating the double integral yields $\mu_0^{\mathrm{CD}} = 1$. In contrast to Eq. (29), the heuristic concentration field in Eq. (31) thus ensures that for $D > 0$ all the injected tracer formally leaves the outlet plane though $(\partial C_{\mathrm{CD}}/\partial R)|_{R=1} < 0$. Inserting Eq. (31) with $Z = 1$ into Eq. (5) yields the mixing cup concentration corresponding to the RTD of the CD regime as given in Eq. (34). It should be noted that for obtaining this result, weighting of the delta function in Eq. (3) by the velocity profile $u(r)$ is essential (Levenspiel et al., 1970; Levenspiel and Turner, 1970). Inserting Eq. (31) with $Z = 1$ into Eq. (6) yields

$$\begin{aligned} \mu_1^{\mathrm{CD}}(\alpha,b) &= \lim_{b\to 0}\frac{1}{2}\int_b^2\left\{\int_0^\infty \sqrt{\frac{\theta}{\pi}}\cdot\alpha V\cdot\exp\left[-\alpha^2\frac{(1-V\theta)^2}{\theta}\right]\cdot\mathrm{d}\theta\right\}\cdot V\cdot\mathrm{d}V \\ &= 1+\lim_{b\to 0}\left[\frac{1}{4\alpha^2}\ln\left(\frac{2}{b}\right)\right] \end{aligned} \tag{32}$$

and $\mu_2^{\mathrm{CD}} = \infty$. These results imply that the reduced mean RT becomes 1 in the limit $\alpha\to\infty$ while the reduced variance is infinite.

By replacing the spatial delta function by a regularized version with

exponential term, we thus have derived the following outlet concentration of the convection dominated (CD) regime

$$C_{\text{out}}^{\text{CD}}(\theta|\alpha,V)=\frac{\alpha}{\sqrt{\pi\theta}}\cdot V\cdot\exp\left[-\alpha^2\frac{(1-V\theta)^2}{\theta}\right], \tag{33}$$

where $V=2(1-R^2)$ represents the normalized Poiseuille velocity profile. The resulting RTD of the convection dominated regime is obtained as

$$E_\theta^{\text{CD}}(\theta|\alpha)=\frac{1}{2\theta^3}\left\{\frac{\sqrt{\theta}}{2\sqrt{\pi}\,\alpha}\left[\exp\left(-\frac{\alpha^2}{\theta}\right)-(1+2\theta)\cdot\exp\left(-\alpha^2\frac{(1-2\theta)^2}{\theta}\right)\right],\right.$$
$$\left.+\frac{2\alpha^2+\theta}{4\alpha^2}\left[\text{erf}\left(\frac{\alpha}{\sqrt{\theta}}\right)-\text{erf}\left(\alpha\frac{1-2\theta}{\sqrt{\theta}}\right)\right]\right\} \tag{34}$$

where $\text{erf}(x)=2\pi^{-1/2}\int_0^x e^{-t^2}dt$ denotes the error function. In the limit $\alpha\to\infty$, Eq. (34) reduces to the correct pure convection RTD for laminar pipe flow of a Newtonian fluid according to Eq. (19).

In Fig. 2 we compare the RTD from Eq. (34) for three different values of α. For $\alpha=125$, Eq. (34) is visually identical to the exact pure convection RTD in Eq. (19). With decrease of α corresponding to an increase of D the first effect reported by Bosworth (1948) is observed. Namely, the sharp cut-off of at $\theta_f=0.5$ is replaced by a more gradual one while some molecules have a residence time less than θ_f. The second effect of diffusion reported by Bosworth (1948), i.e. the flattening of the RTD curve at high values of θ, becomes visible only for the smallest value of α.

3.1.3. Postulated outlet concentration field

To combine the outlet concentration field of the AD regime, Eq. (23), with that of the CD regime, Eq. (33), we postulate the following outlet concentration field for the transition regime

$$C_{\text{out}}^{\text{MTR}}(\theta|V,p,S)=\frac{1-p+pV}{\sqrt{2\pi S\theta}}\cdot\exp\left\{-\frac{[1-\theta(1-p+pV)]^2}{2S\theta}\right\} \tag{35}$$

This particular outlet concentration field is chosen because it allows to carry out all integrations in the various equations in Section 2.2.3 analytically. In Eq. (35), $p=p(\alpha)$ is a regime transition parameter in the range $0\le p(\alpha)\le 1$ (cf. black arrow in Fig. 1 a) while $S=S(\alpha)>0$ is a parameter related to the variance of the RTD. Eq. (35) reduces for $p=0$ and $S=\alpha/24$ to the transversal uniform outlet concentration of the axial dispersion model with spatial delta pulse, Eq. (23). For $p=1$ and $S=1/2\alpha^2$, Eq. (35) reduces to the outlet concentration field of the convection dominated regime based on a regularized spatial delta pulse, Eq. (33). While the outlet concentration field in Eq. (35) satisfies the condition of vanishing radial gradient at the pipe axis, the boundary condition of an impermeable tube wall is not fulfilled. In the following it will be necessary to restrict the transition parameter to the range $0<p<1$. The parameter p enables a smooth transition of the skewed PC RTD ($p\to1$) towards the symmetric Gaussian RTD of the AD regime in the limit $p\to0$.

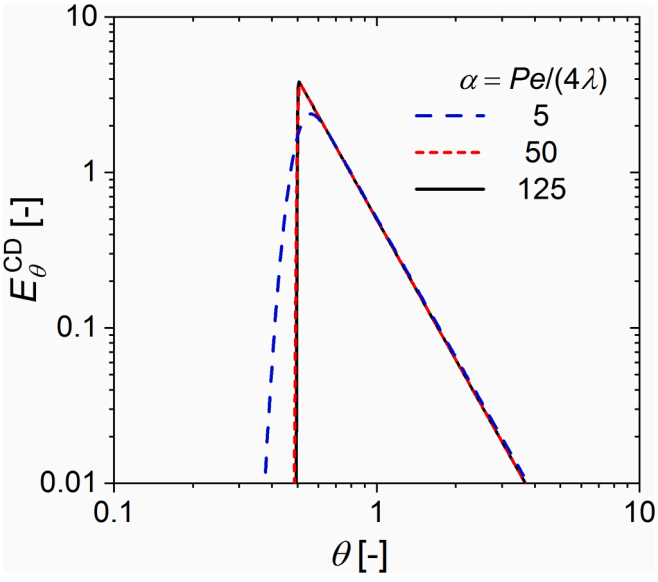

Fig. 2. Log-log plot of normalized RTD curves for the convection dominated model as given by Eq. (34) for three different values of α.

Inserting the assumed outlet concentration profile from Eq. (35) into Eq. (6), taking $n=0$ and evaluating the integral yields for the zero moment the result $\mu_0^{\text{MTR}}=1$, see Supplemental Material Section 3.1. All tracer injected at the inlet plane thus leaves the outlet plane, independent on the values of p and S. This results in the relationships $E_\theta^{\text{MTR}}=C_{\text{cup}}^{\text{MTR}}$, $\bar{\theta}_{\text{MTR}}=\mu_1^{\text{MTR}}$ and $\sigma_{\theta,\text{MTR}}^2=\mu_2^{\text{MTR}}-\bar{\theta}_{\text{MTR}}^2$, cf. Eqs. (7)–(9).

3.1.4. Unclosed MTR model

Inserting the assumed outlet concentration profile from Eq. (35) into Eq. (5) and evaluation of the integral by assuming $p>0$ yields $E_\theta^{\text{MTR}}(\theta|p,S)=C_{\text{cup}}^{\text{MTR}}(\theta|p,S)$ as given by Eq. (S.3) in Supplemental Material. With the abbreviation $f_\pm=(1-\theta\pm p\theta)/\sqrt{2S\theta}$ one can express the unclosed RTD as

$$E_\theta^{\text{MTR}}(\theta|p,S)=\frac{1}{2\theta^3}\left\{\sqrt{\frac{S\theta}{2\pi}}\,\frac{\exp\,(-f_+^2)-(1+2p\theta)\exp\,(-f_-^2)}{p^2}+[1-\theta(1\right.$$
$$\left.-p-S)]\frac{\text{erf}\,(f_+)-\text{erf}\,(f_-)}{2p^2}\right\} \tag{36}$$

The pre-factor $1/2\theta^3$ in Eq. (36) also occurs in the RTD of the pure convection regime, Eq. (19). The deviation of the terms in the curly brackets from the Heaviside function in Eq. (19) thus represents the deviation of the RTD in the transition regime from that of the PC regime. Profiles of the four terms in Eq. (36) for different values of p in combination with Eq. (42) for S as derived below are shown in the Supplemental Material (Fig. S.2). The mathematical structure of Eq. (36) is similar to the analytical RTD obtained by neglecting radial diffusion in Eq. (2) while retaining axial diffusion, see Platzer et al. (1999, Eq. (36)) and Fazli-Abukheyli & Darvishi (2019, Eq. (13)).

Inserting the assumed outlet concentration profile from Eq. (35) into Eq. (6), taking $n=1$ and calculation of the integral yields for the mean value of the RTD the result

$$\bar{\theta}_{\text{MTR}}(p,S)=\mu_1^{\text{MTR}}(p,S)=\frac{1+p-S}{p+p^2}-\frac{1-p-S}{p^2}\text{Arctanh}(p), \tag{37}$$

see Supplemental Material Section 3.2. The definition range of the inverse hyperbolic function requires the restriction $p<1$. Repeated application of L'Hôspital's rule to Eq. (37) yields the limits

$$\lim_{p\to0}\mu_1^{\text{MTR}}(p,S)=1+S,\quad \lim_{p\to1}\mu_1^{\text{MTR}}(p,S)=1+\lim_{p\to1}(S\cdot\text{Arctanh}(p)) \tag{38}$$

The condition $\mu_1^{\text{MTR}}\ge1$ thus requires $S(p)\ge0$.

Inserting the assumed outlet concentration profile from Eq. (35) into Eq. (6), taking $n=2$ and calculation of the integral yields for the second moment about the origin the result

$$\mu_2^{\text{MTR}}(p,S)=\frac{\text{Arctanh}(p)}{p^2}-\frac{1}{1+p}\left\{\frac{1}{p}-\frac{S}{1-p^2}\left(3+\frac{3-p}{1-p^2}S\right)\right\}, \tag{39}$$

see Supplemental Material Section 3.3. The reduced variance is obtained by inserting Eq. (37) and Eq. (39) into $\sigma_{\theta,\text{MTR}}^2=\mu_2^{\text{MTR}}-\bar{\theta}_{\text{MTR}}^2$, see Supplemental Material Eq. (S.16). The cumulative RTD of the unclosed MTR

model is derived in Supplemental Material Section 3.4.

To close the MTR model, we need to express p and S as functions of the normalized transversal diffusion time α. To that end we first determine the relation $S = S(p)$ and thereafter the relation $p = p(\alpha)$. To determine parameter S, we resort to the result for the mean value of the unclosed RTD in Eq. (37). For an ideal delta pulse in time the mean value of the solute RTD equals the mean value of the solvent RTD, i.e., the space time. For an open-open system, the mean value of the RTD of the solute is typically slightly larger than that of the solvent (Spalding, 1958). We thus require at this stage of model development $\overline{\theta}_{\mathrm{MTR}} \geq 1$.

Setting $\overline{\theta}_{\mathrm{MTR}}$ in Eq. (37) to 1 yields the relation

$$S_{\mathrm{mean}\,=\,1}(p) = \frac{(1-p^2)[\mathrm{Arctanh}\ (p) - p]}{(1+p)\mathrm{Arctanh}\ (p) - p}, \tag{40}$$

which is plotted in Fig. 3. The curve $S_{\mathrm{mean}=1}(p)$ has a maximum value 0.1173 at $p = 0.5826$ and the analytical limits

$$\lim_{p\to 0} S_{\mathrm{mean}\,=\,1}(p) = \lim_{p\to 1} S_{\mathrm{mean}\,=\,1}(p) = 0 \tag{41}$$

To meet the limits $S(p{\to}0) = \alpha_{\mathrm{AD}}/24$ and $S(p{\to}1) = 1/2\alpha_{\mathrm{CD}}^2$ of the AD and CD regimes, we set

$$S(p,k) = \frac{\alpha_{\mathrm{AD}}}{24}(1-p) + \frac{p}{2\alpha_{\mathrm{CD}}^2} + k\cdot\frac{(1-p^2)[\mathrm{Arctanh}\ (p) - p]}{(1+p)\mathrm{Arctanh}\ (p) - p}, \tag{42}$$

where $0 \leq k \leq 1$ so that $S(p) > 0$ for $0 < p < 1$. The parameter k is introduced to allow the choice between two models for the RTD in the transition regime. Each of the two models has its own limitations, which are explained below.

At this stage it is necessary to select specific values for α_{AD} and α_{PC} to proceed. However, the development of the present analytical model is such that both parameters can be easily changed if necessary. Taking the diagonal lines of the hatched transition regime in Fig. 1(a) as limits it is $\alpha_{\mathrm{AD}} = 0.25$ and $\alpha_{\mathrm{PC}} = 125$ so that $S(p=0) = 1/96$ and $S(p=1) = 1/31250$. The resulting relation $S(p)$ is plotted in Fig. 3 for two different values of k. For $k = 1$, the maximum value $S_{\mathrm{max}} = 0.1217$ is obtained for $p = 0.5716$; for $k = 1-p$ the maximum value $S_{\mathrm{max}} = 0.0684$ is lower and obtained for $p = 0.3683$.

By inserting $S = S(p,k)$ from Eq. (42) into Eq. (36), we can now plot for either value of k continuous families of curves $E_\theta^{\mathrm{MTR}}(\theta|p,k)$ with sole parameter p. Fig. 4 shows the corresponding set of curves for nine

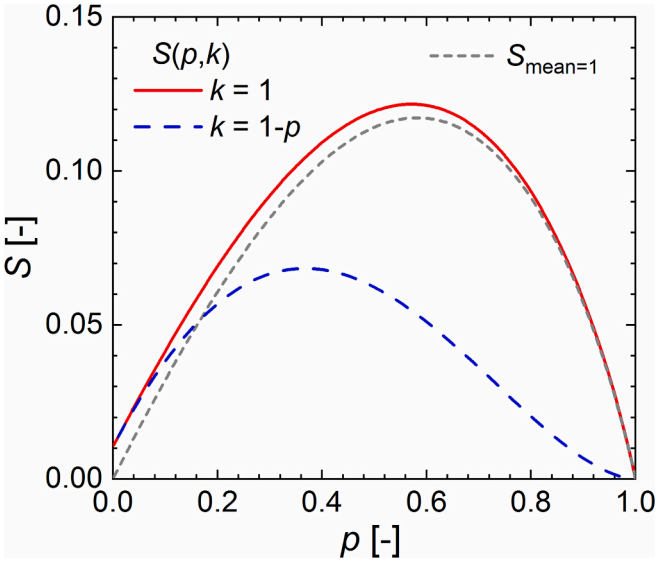

Fig. 3. Plots of $S_{\mathrm{mean}=1}(p)$ and of $S(p,k)$ for $k = 1$ and $k = 1-p$ as given by Eq. (40) and Eq. (42), respectively, in combination with $\alpha_{\mathrm{AD}} = 0.25$ and $\alpha_{\mathrm{PC}} = 125$.

different values of p in the range 0.001 –0.999. With increase of p, the differential RTD curves change from the symmetric Gaussian bell shape of the AD regime to the skewed RTD of the PC regime, with the position of the RTD maximum shifting from $\theta = 1$ to $\theta = 0.5$. The set of RTD curves $E_\theta^{\mathrm{MTR}}(\theta|p,k=1)$ in Fig. 4(a) exhibits two weaknesses. First, even for $p = 0.999$ the maximum value 3.44 of the RTD is notably below the maximum value 4 of the PC regime. Second, the RTD curves for $p > 0.1$ have non-zero (positive) values for $\theta < \theta_{\mathrm{f}} = 0.5$ which means that some tracer reaches the outlet plane faster than the fastest solvent molecules. Since longitudinal molecular diffusion is neglected in the derivation as it is insignificant in the considered parameter range of Pe and λ, such behavior is inconsistent with model assumptions and essentially unphysical.

Both of the latter weaknesses can be mitigated by setting $k = 1-p$, as shown in Fig. 4(b). The maximum value of the RTD for $p = 0.999$ is now increased to 3.84. Furthermore, the relative fraction of tracer with residence time below $\theta_{\mathrm{f}} = 0.5$ is significantly reduced. For values $p < 0.1$ the differences in the RTD curves in Fig. 4(a) and (b) are very small. The choice $k = 1-p$ makes the RTD curves for $p > 0.25$ physically more plausible, but goes along with a drawback regarding the mean RT as discussed next.

Inserting Eq. (42) into Eq. (37) yields for the mean RT of the MTR model the result

$$\overline{\theta}_{\mathrm{MTR}}(p,k) = \frac{1-k(1-p)}{p} - \frac{(1-p)(1-k)}{p^2}\mathrm{Arctanh}(p) - \left(\frac{\alpha_{\mathrm{AD}}}{24}(1-p) + \frac{p}{2\alpha_{\mathrm{CD}}^2}\right)\frac{p-(1+p)\mathrm{Arctanh}(p)}{p^2(1+p)} \tag{43}$$

Eq. (43) is plotted in Fig. 5 for the two different values of k. For $k = 1$, the mean solute RT decreases monotonically with increase of p, but is always larger than 1. For $k = 1-p$, however, the mean RT of the solute is not monotonic and takes values less than 1 for $p > 0.167$. The minimum value of the mean RT of 0.927 is obtained for $p = 0.7885$.

In reality, the mean RT measured by inert tracer experiments may be smaller than the space time of the reactor due to the existence of stagnation or recirculation zones. In the present theoretical approach, such zones are excluded because the parabolic velocity profile is assumed. In practice, measured tracer data for times longer than 2–3 space times are seldom accurately enough to be used for RTD calculations (Bischoff and McCracken, 1966). For calculating the mean RT and the variance, the integrals in Eq. (8) and Eq. (9) are therefore often truncated by replacing the upper limit of integration of infinity by $\theta = 2$ or 3. Accordingly the truncated mean RT from tracer measurements can be lower than the space time, see e.g. Gobert et al. (2017, Table 4), where the measured mean RT is up to 10 % smaller than the expected mean RT. For non-inert matter it is known that irreversibly absorbing analytes move faster than inert analytes in pressure-driven flow. This is because the slow-moving analyte molecules near the wall are preferentially removed from the channel (Datta and Ghosal, 2009; Sankarasubramanian and Gill, 1973). Correspondingly, the mean RT of the solute is lower than the mean RT of the solvent.

Inserting Eq. (37) and Eq. (39) in combination with Eq. (42) into $\sigma_{\theta,\mathrm{MTR}}^2 = \mu_2^{\mathrm{MTR}} - \overline{\theta}_{\mathrm{MTR}}^2$ yields the reduced variance of the MTR model which is for $k = 1$ and $k = 1-p$ plotted in the inset of Fig. 6. For both values of k, the minimum value of the variance is obtained in the limit $p{\to}0$. The minimum value $49/4608 \approx 0.01063$ is in agreement with the variance of the AD model for $\alpha = \alpha_{\mathrm{AD}} = 0.25$. By Eq. (42), the variance-related parameter $S(p,k)$ decreases with decrease of k. Choosing $k = 1-p$ therefore reduces the variance as compared to the case $k = 1$, see inset of Fig. 6. For both choices of k, the variance increases monotonically with increasing p and becomes infinite in the limit $p{\to}1$. Although other choices for k besides $k = 1$ and $k = 1-p$ are possible and have been tested, these have not proven to be useful.

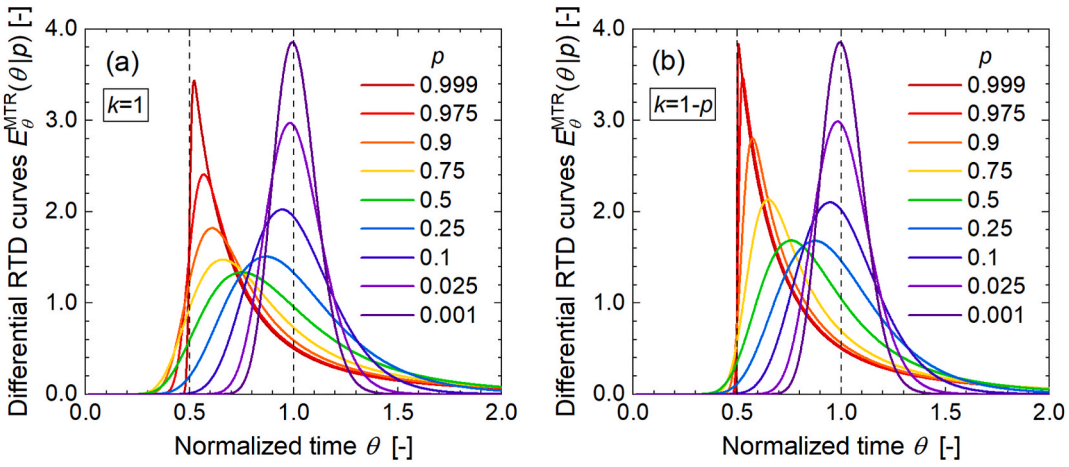

Fig. 4. Families of RTD curves of the MTR model under variation of the regime transition parameter p for $k = 1$ (a) and $k = 1 - p$ (b). Regime boundaries are $\alpha_{AD} = 0.25$ and $\alpha_{PC} = 125$.

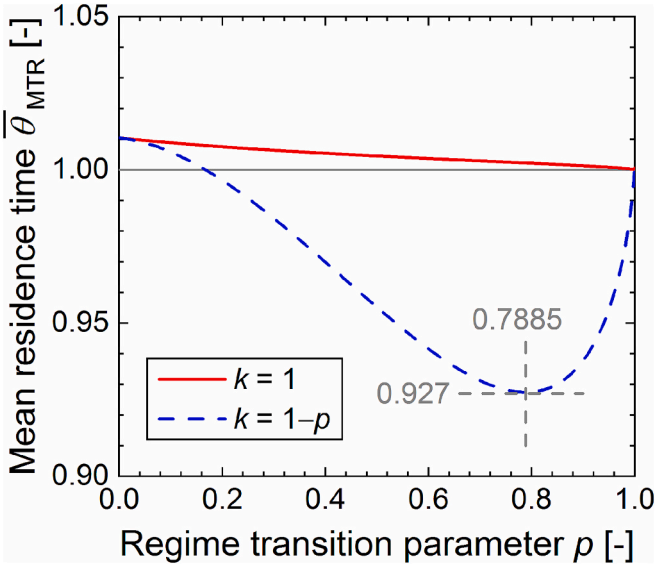

Fig. 5. Mean normalized solute residence time $\overline{\theta}_{MTR}(p,k)$ of the MTR model as function of regime transition parameter p for $k = 1$ and $k = 1 - p$. Regime boundaries are $\alpha_{AD} = 0.25$ and $\alpha_{PC} = 125$.

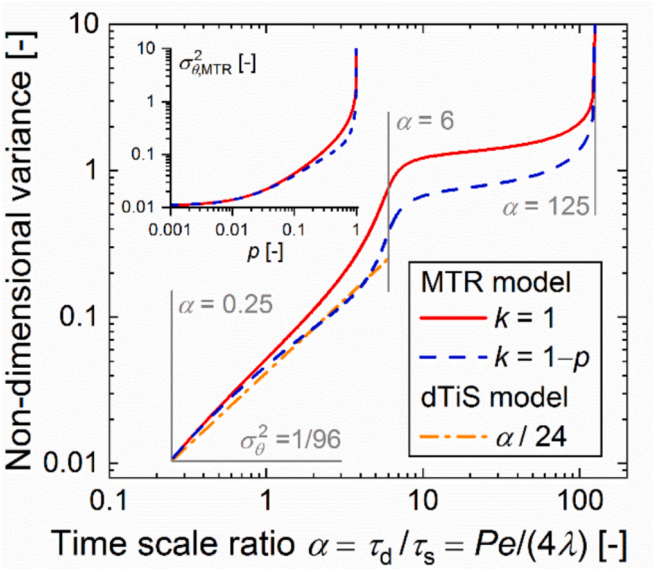

Fig. 6. Non-dimensional reduced variance of the MTR and dTiS models as function of α (main graph), and of regime transition parameter p (inset, MTR model only). Regime boundaries are $\alpha_{AD} = 0.25$ and $\alpha_{PC} = 125$.

3.2. Compartment model (dTiS model)

While the MTR model given by Eq. (36) and Eq. (42) has the advantage of being derived from first principles, its complexity may appear as a disadvantage. Furthermore, the computational evaluation can cause numerical underflows for very small values of the arguments of the exponential function. We therefore present a phenomenological compartment model as simpler alternative. Compartment models are based on the combination of ideal CSTR and PFR arranged in different configurations (Levenspiel, 1999). In the present case the compartment model consists of one PF unit followed by a cascade of ideally mixed CSTR's with equal volumes and identical flow rates, a model that is already used in the context of hot melt extrusion (Grimard et al., 2016), powder blending (Escotet-Espinoza et al., 2019) and constructed wetlands (Zhang et al., 2024).

The dimensional RTD of a cascade of $n = 1, 2, 3, \cdots$ equal-volume CSTRs in series with mean residence time $\bar{t}_{TiS}$ is (MacMullin and Weber, 1935)

$$E_{TiS}(t|n) = \frac{n^n}{(n-1)!}\frac{t^{n-1}}{\bar{t}_{TiS}^{\,n}}\exp\left(-\frac{nt}{\bar{t}_{TiS}}\right) \tag{44}$$

This tank-in-series (TiS) model can be generalized to the extended tank-in-series (eTiS) model (Martin, 2000) with non-dimensional RTD

$$E_\theta^{eTiS}(\theta|q) = \frac{q^q}{\Gamma(q)}\theta^{q-1}\exp(-q\theta) \tag{45}$$

Here, $\Gamma(q)$ denotes the (complete) Gamma function, with q being a positive real number that removes the problem of quantization (Buffham and Gibilaro, 1968) which occurs as n tends to 1 in Eq. (44).

Here, we consider a compartment model where a PFR is in series with an eTiS. Due to the PFR, material reaches the eTiS with a delay time t_D so that the RTD from Eq. (44) becomes

$$E_{dTiS}(t|q) = \begin{cases} 0 & t < t_D \\ \dfrac{q^q}{\Gamma(q)}\dfrac{(t-t_D)^{q-1}}{\bar{t}_{eTiS}^{\,q}}\exp\left(-q\dfrac{t-t_D}{\bar{t}_{eTiS}}\right) & t \geq t_D \end{cases} \tag{46}$$

The mean value of this RTD is $\bar{t}_{\mathrm{dTiS}} = t_{\mathrm{D}} + \bar{t}_{\mathrm{eTiS}}$ so that the non-dimensional RTD becomes

$$E_{\theta}^{\mathrm{dTiS}}(\theta|q,\theta_{\mathrm{D}}) = \begin{cases} 0 & \theta < \theta_{\mathrm{D}} \\ \dfrac{1}{1-\theta_{\mathrm{D}}}\dfrac{q}{\Gamma(q)}\left(q\dfrac{\theta-\theta_{\mathrm{D}}}{1-\theta_{\mathrm{D}}}\right)^{q-1}\exp\left(-q\dfrac{\theta-\theta_{\mathrm{D}}}{1-\theta_{\mathrm{D}}}\right) & \theta \geq \theta_{\mathrm{D}} \end{cases} \tag{47}$$

The delay time associated with PF behavior is considered equal to the first appearance time $\theta_{\mathrm{f}} = 0.5$ of Poiseuille flow. Assuming $t_{\mathrm{D}} = \bar{t}_{\mathrm{eTiS}} = \tau_{\mathrm{s}}/2$ so that $\theta_{\mathrm{D}} = t_{\mathrm{D}}/\bar{t}_{\mathrm{dTiS}} = 0.5$ yields the delayed-tank-in-series (dTiS) model with differential and cumulative RTD given by

$$E_{\theta}^{\mathrm{dTiS}}(\theta|q) = H(\theta-0.5)\cdot\frac{2q^{q}}{\Gamma(q)}(2\theta-1)^{q-1}\exp[-q(2\theta-1)], \tag{48}$$

$$F^{\mathrm{dTiS}}(\theta|q) = H(\theta-0.5)\cdot\left(1-\frac{\Gamma(q,q(2\theta-1))}{\Gamma(q)}\right) \tag{49}$$

Here $\Gamma(q,x) = \int_x^{\infty} t^{q-1}e^{-t}dt$ denotes the upper incomplete Gamma function so that $\Gamma(q,0) = \Gamma(q)$. Since Eq. (48) becomes infinite in the

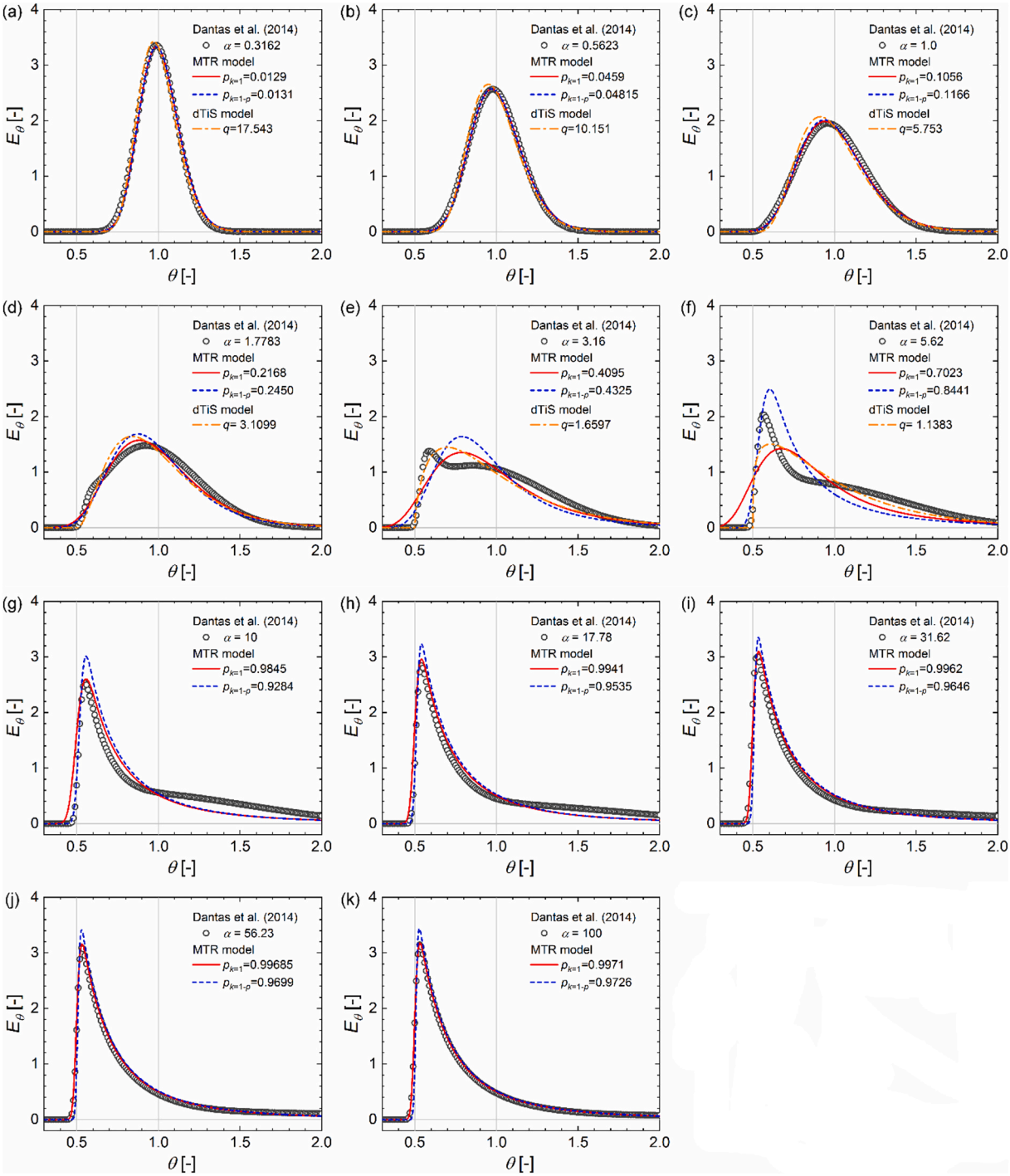

Fig. 7. In the eleven subfigures (a-k), open circle symbols represent the numerical RTD data of Dantas et al. (2014) for eleven different values of α. Lines represent least-squares fits of parameter p of the MTR model, Eq. (36), and of parameter q of the dTiS model, Eq. (48), to the numerical RTD data. Parameter S of the MTR model is given by Eq. (42) and fits are performed for $k = 1$ and $k = 1-p$. Obtained fit values for p and q for each value of α are given in the legend of each subfigure.

limit $\theta \to +0.5$ for $q < 1$ we restrict the number of hypothetical tanks in series to $q \geq 1$. The mean value of $E_\theta^{\mathrm{dTiS}}(\theta|q)$ is 1 and the variance is $1/4q$. The inset in Fig. 9 shows RTD curves for six different values of q. In the limit $q \to \infty$ plug flow is approached. The one-parameter RTD curves $E_\theta^{\mathrm{dTiS}}(\theta|q)$ can be considered as a special case of the general three-parameter gamma distribution model (Johnson et al., 1971; Wen and Fan, 1975) in absence of bypass flow and in combination with a dimensionless delay time 0.5 of the plug flow section.

3.3. Model closure

To close the MTR and dTiS models, the regime transition parameters p and q have to be related to the normalized transversal diffusion time $\alpha = Pe/4\lambda$. For this purpose, we resort to numerical solutions of the non-dimensional advection–diffusion equation in the absence of axial diffusion, Eq. (20) with present normalization. While there are early numerical solutions obtained with different normalizations (Shankar and Lenhoff, 1989, 1991), we use here more recent numerical results of Dantas et al. (2014) which are based on the present normalization.

3.3.1. Fit of one-parameter models to numerical RTD data

Eq. (20) is a special case (Newtonian fluid) of a more general equation in Dantas et al. (2014, Eq. (13)) for non-Newtonian power-law fluids, where α is denoted as modified Peclet number (Pe'). The authors solved Eq. (20) for different values of α numerically by a finite difference method in combination with a step input (Dantas et al., 2014). From the numerical results for the mixing cup average tracer concentration at the outlet plane, sampled values of the cumulative distribution function $F_i(\theta_i)$ were evaluated in intervals $\Delta\theta = 0.02$. The discrete differential RTD is obtained as central difference $E_{\theta,i} = (F_{i+1} - F_{i-1})/2\Delta\theta$. The numerical E-curves of laminar flow with radial diffusion in a straight tube obtained in this way were used for characterizing measured RTD curves in a holding tube with U-bend. The total of 17 considered values for α span the range from $\log(\alpha) = -1.5$ to $\log(\alpha) = 2.5$ where steps of $\log(\alpha) = 0.25$ are employed, corresponding to the range $0.0316 \leq \alpha \leq 316$. Since the four smallest values of α are lower than $\alpha_{\mathrm{AD}} = 0.25$ while the two highest values are larger than $\alpha_{\mathrm{PC}} = 125$, we use here numerical data for eleven different values of α in the range $-0.5 \leq \log(\alpha) \leq 2$ only, corresponding to $0.0316 \leq \alpha \leq 100$. Fig. 7 shows for these eleven values of α least-square fits of the MTR model to the numerical results of Dantas et al. (2014), both for $k = 1$ and $k = 1 - p$. For the dTiS model, only fits to numerical data for $\alpha \leq 5.62$ are displayed in Fig. 7 because larger α values lead to values $q < 1$, which we do not allow here.

The fitting of the numerical RTD data of Dantas et al. (2014) for the MTR model in Fig. 7(a-k) is done with Mathematica Software (version 12) using FindFit[*data*,(*expr*,*cons*),*pars*,*vars*]. This built-in Mathematica symbol function finds numerical values of the parameters *pars* that make *expr* under the constraints *cons* give a best least-squares fit to *data* as a function of *vars*. Here, the range of *data* is restricted so that only RTD values satisfying $E_{\theta,i}(\theta_i) > 5{\cdot}10^{-7}$ are considered for the fit. For *expr*, the mathematical relationship defining the MTR model either with $k = 1$ or $k = 1 - p$ is used in combination with the constraint $0 < p < 1$. The two remaining arguments *pars* and *vars* are given by p and θ, respectively. For the fitting of the numerical RTD data of Dantas et al. (2014) in Fig. 7 (a-f) to the dTiS model, the software OriginPro 2019 (Version 9.6.0.172) is used in combination with a user defined function representing Eq. (48) and the Levenberg-Marquardt algorithm. With increase of α from 0.316 to 4.62, the coefficient of determination R^2 decreases from 0.996 to 0.95. We also fitted the MTR model to the entire range of the cumulative RTD $F_i(\theta_i)$, which lead to different results as compared to the fit using the range-restricted differential RTD. However, the values of p obtained by fit of the cumulative RTD did not yield a good agreement between the respective curve of the MTR model and the corresponding numerical differential RTD.

3.3.2. Predictive models for the RTD in the transition regime

By the described procedure, eleven discrete data pairs for $p_i(\alpha_i)$ and six discrete data pairs for $q_i(\alpha_i)$ are obtained, which are shown in Fig. 8 and Fig. 9, respectively. Fig. 8 shows that for both, $\alpha < 6$ and $\alpha > 6$ the relationship $p = p(\alpha)$ in the MTR model is close to linear. However, since the slope in both regions is very different, the overall relation is strongly non-linear. A suitable model for data that follow two different linear relationships but allow for a smooth transition from one linear regime to the other is the "bent-hyperbola" regression model (Griffiths and Miller, 1973). To fit the data $p_i(\alpha_i)$ in Fig. 8, we resort to a parametrization of the bent-hyperbola model (Ratkowsky, 1990, Eq. (4.5.6)). This five-parameter model, made up of two intersecting straight lines as a limiting case, is given by the equation

$$p(\alpha|c_1,c_2,c_3,c_4,c_5) = c_1 + c_2(\alpha - c_4) - c_3\sqrt{(\alpha - c_4)^2 + c_5^2} \tag{50}$$

By the condition $p(0.25) = 0$ the parameter c_1 is determined as

$$c_1 = c_2(c_4 - 0.25) + c_3\sqrt{(c_4 - 0.25)^2 + c_5^2} \tag{51}$$

while the condition $p(125) = 1$ yields

$$c_2 = \frac{1 + c_3\sqrt{(125 - c_4)^2 + c_5^2} - c_3\sqrt{(c_4 - 0.25)^2 + c_5^2}}{125 - 0.25}, \tag{52}$$

resulting in the three-parameter model

$$\begin{aligned} &p(\alpha|c_3,c_4,c_5) \\ &= \frac{\alpha - 0.25}{125 - 0.25}\left[1 + c_3\sqrt{(125 - c_4)^2 + c_5^2} - c_3\sqrt{(c_4 - 0.25)^2 + c_5^2}\right] \\ &\quad - c_3\sqrt{(\alpha - c_4)^2 + c_5^2} + c_3\sqrt{(c_4 - 0.25)^2 + c_5^2} \end{aligned} \tag{53}$$

Since the differences in the data points for $k = 1$ and $k = 1 - p$ in Fig. 8 are rather small, the relation $p = p(\alpha)$ in the MTR model is here approximated independent on both alternatives for k by a common fit. Furthermore, to keep the relation $p(\alpha)$ relatively simple, the remaining parameters are not obtained by a regression. Instead, they are arbitrarily set to rounded values $c_3 = 1/12$, $c_4 = 6$ and $c_5 = 1$ to obtain

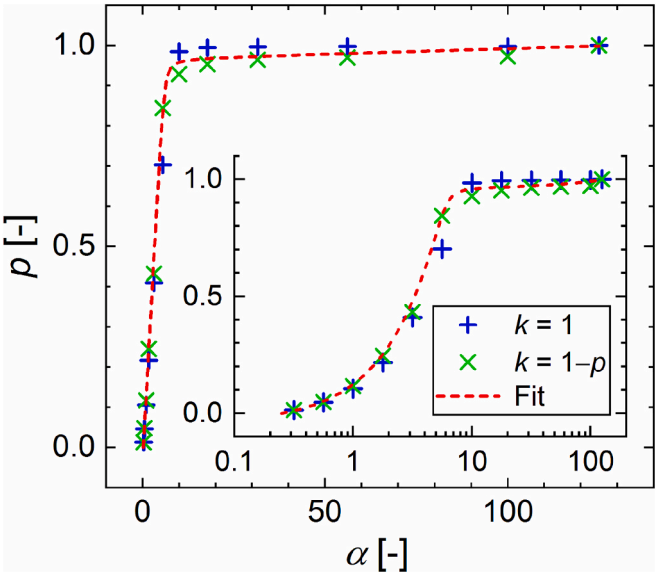

Fig. 8. Relationship $p(\alpha)$ for the MTR model in linear (main graph) and log-linear (inset) representation. The symbols correspond to the least-squares fit values given in the legends of Fig. 7(a-k).

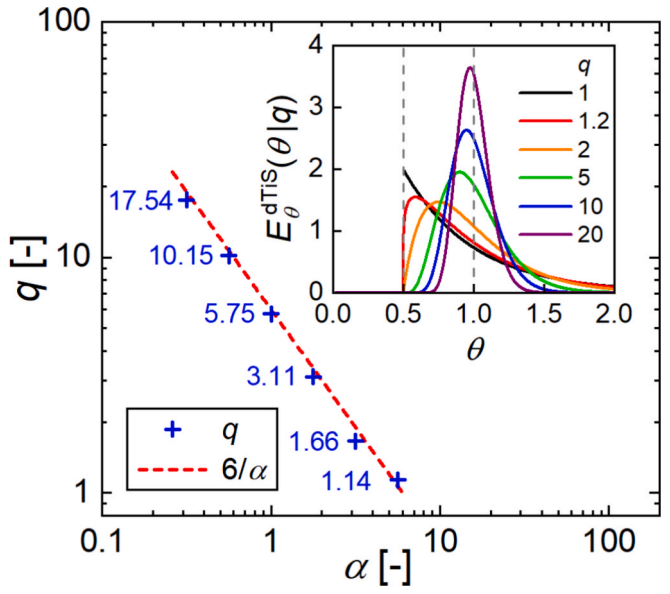

Fig. 9. Relationship $q(\alpha)$ for the dTiS model with the inset showing typical E_θ-curves for different values of q. The symbols in the main graph correspond to the least-squares fit values given in the legends of Fig. 7(a-f).

$$p(\alpha) = \underbrace{\frac{125\sqrt{545} - \sqrt{14162} - 12}{5988}}_{\approx 0.4655} + \underbrace{\frac{48 + 4\sqrt{14162} - \sqrt{545}}{5988}}_{\approx 0.0836}\cdot\alpha - \frac{\sqrt{1 + (\alpha - 6)^2}}{12}, \tag{54}$$

where $0.25 < \alpha < 125$.

The latter relationship completes the present mechanistic transition regime (MTR) model, which is given by Eqs. (36), (42) and (54). The value of k should be chosen as a compromise depending which model weakness is more acceptable. If the violation of the breakthrough time 0.5 is acceptable, then the value $k = 1$ is recommended as it ensures that the mean solute RT given by Eq. (43) is slightly larger than the space time. On the other hand, if a violation of the breakthrough time 0.5 is not acceptable while a mean solute RT lower than the space time is tolerable, then it is recommended to use the value $k = 1 - p$ in Eq. (42) for $S = S(p, k)$.

For the dTiS model, the symbols in Fig. 9 can well be fitted by the simple relationship $q(\alpha) = 6/\alpha$. The final differential and cumulative RTDs of the dTiS model with mean value 1 and variance $\alpha/24$ then become

$$E_\theta^{dTiS}(\theta|\alpha) = \frac{H(\theta - 0.5)}{\Gamma(6/\alpha)}\cdot\frac{12}{\alpha}\cdot\left[\frac{6(2\theta - 1)}{\alpha}\right]^{\frac{6-\alpha}{\alpha}}\cdot\exp\left[-\frac{6(2\theta - 1)}{\alpha}\right] \tag{55}$$

and

$$F_{dTiS}(\theta|\alpha) = H(\theta - 0.5)\cdot\left[1 - \frac{\Gamma(6/\alpha, 6(2\theta - 1)/\alpha)}{\Gamma(6/\alpha)}\right], \tag{56}$$

respectively, where $0.25 \le \alpha \le 6$.

4. Discussion

4.1. Straight tubes

To the author's knowledge, the MTR and dTiS models developed in Section 3 represent the first models for the RTD in the transition regime. The MTR model is valid in the entire hatched region in Fig. 1(a) and covers with the range $0.25 < \alpha < 125$ almost three orders of magnitude in α. The dTiS model is only applicable in a subset of the hatched area of Fig. 1 (a), as its validity range $0.25 \le \alpha \le 6$ is much smaller. Since the normalized transversal diffusion time $\alpha = a^2U/LD = Pe/4\lambda$ is usually known in advance, both RTD models are predictive for straight tubes with operating conditions falling in the transition regime.

For the MTR model, it should be emphasized that the postulated outlet concentration distribution in Eq. (35) is only a heuristic approximation. Since the radial gradient of the assumed concentration distribution in the outlet plane at the pipe wall is non-zero, it is not compatible with the advection–diffusion equation given by Eq. (20) in combination with a zero mass-flux condition at the tube wall. In the limit $\alpha \to \alpha_{AD} = 0.25$ this model deficiency is not of great relevance as the wall concentration gradient in Eq. (35) becomes very small in accordance to the transversally uniform concentration field of the underlying limit of the AD regime. In the limit $\alpha \to \alpha_{PC} = 125$, the model deficiency is probably of no great practical relevance as well, as the area of the thin annular region where the concentration gradient at the wall vanishes should be very small as compared to the pipe cross-section. It is therefore expected that disregarding the no-mass flux boundary condition may in the limit $\alpha \to \alpha_{PC}$ mainly affect the tail of the RTD. Fig. 7(a) and Fig. 7(k) confirm that the RTDs predicted by the MTR model on basis of the postulated outlet concentration distribution in Eq. (35) agree in the limits $\alpha \to \alpha_{AD} = 0.25$ and $\alpha \to \alpha_{PC} = 125$ indeed very well with the RTDs obtained by numerical solution of Eq. (20) by Dantas et al. (2014) in combination with a zero mass-flux condition at the tube wall. Concerning the tail of skew RTDs it is also interesting to mention findings of a recent study on pharmaceutical manufacturing, which showed that the tails of experimental RTDs can be truncated with no loss of accuracy from quality assurance perspective (Bhalode et al., 2023).

The error made by disregarding the non-penetration condition at the wall seems to be largest for $2 < \alpha < 8$. In this range of the time scale ratio τ_d/τ_s, the numerical RTDs exhibit a right-skewed "platform" or plateau as shown in Fig. 7(e) and Fig. 7(f). The origin of the plateau in the RTD lies in plateaus or double-humped peaks that occur in concentration-over-time curves under certain conditions, where radially inward diffusion of solute from low velocity regions near the pipe wall towards the axis coexists with radially outward diffusion from the high velocity region at the pipe axis (Gill and Ananthakrishnan, 1967; Golay and Atwood, 1979; Guan and Chen, 2024; Korenaga et al., 1989a; Korenaga et al., 1989b; Mayock et al., 1980; Shankar and Lenhoff, 1991). Such a plateau region of the RTD, which occurs in a certain range of θ only, where both diffusion regions have not fully interacted, cannot be predicted by either the MTR model or the dTiS model, cf. the set of RTD curves of both models in Fig. 4 and the inset of Fig. 9, respectively. The lacking of this plateau region in the family of RTD curves of the MTR model may be related to the violation of non-penetration boundary condition at the pipe wall. However, despite of several attempts, the author did not find a heuristic outlet concentration distribution that fulfills the non-penetration boundary condition at the tube wall while allowing for analytical calculation of all relevant integrals required for determining the RTD by the novel procedure outlined in this paper.

The dispersion regime map of Levenspiel (1999, Fig. 15.2) suggests to model the RTD in the region of the pure convection regime by Eq. (19). This equation is independent on Pe and λ. An alternative may be to use for $\alpha > 125$, corresponding to the pure convection regime in Fig. 1 (a), Eq. (34) instead, which approaches Eq. (19) in the limit $\alpha \to \infty$. However, already for $\alpha \ge 50$ the difference between Eq. (34) and Eq. (19) is very small (Fig. 2).

The presented original approach for deriving an RTD model for the transition regime from an assumed outlet concentration field can be extended to other laminar velocity profiles representing e.g., the flow of non-Newtonian liquids. For this purpose, the RTD of the pure convection model for Poiseuille flow in Eq. (19) should be replaced by the RTD of the generalized convection model with breakthrough time θ_f as a further parameter (Gutierrez et al., 2010; Wörner, 2010).

4.2. Coiled tubes

The dispersion regime map in Fig. 1(a) and the MTR and dTiS models developed in this paper are valid for straight tubes so far. Coiling of a length of tubing saves not only space but also reduces axial dispersion and narrows the RTD as compared to straight tubes (Koutsky and Adler, 1964). For these reasons and due to their lower costs as compared to chip-based reactors, coil-based reactors are the most used continuous flow reactors. We now show that the MTR and dTiS models can be used to predict the RTD in coiled tubes as well.

The reduction of axial dispersion by coiling due to increased transversal mixing by centrifugal Dean vortices can be quantified by a dispersion reduction factor $\kappa = D_{\mathrm{ax,coiled}}/D_{\mathrm{ax,straight}}$, where $0 < \kappa \leq 1$. The idea to extend the applicability of the present model from straight tubes with normalized transversal diffusion time $\alpha_{\mathrm{straight}} = a^2U/LD$ to coiled tubes is to compute a reduced normalized transversal diffusion time $\alpha_{\mathrm{coiled}} = \kappa{\cdot}\alpha_{\mathrm{straight}}$ that is representative for a coiled tube of identical diameter and length. The RTD of the coiled tube predicted by the present models is then given by

$$E_\theta^{\mathrm{coiled}} = E_\theta^{\mathrm{MTR/dTiS}}\left(\theta\middle|\alpha_{\mathrm{coiled}} = \kappa{\cdot}\alpha_{\mathrm{straigth}}\right) \tag{57}$$

To test the validity and accuracy of this approach, we use experimental RTD data of Gobert et al. (2017). Symbols in Fig. 10 show the measured RTD in a coiled tube with 2.4 mm inner diameter where $\lambda = 829$ and $Pe = 41511$. The value of the normalized transversal diffusion time for the corresponding straight pipe is $\alpha_{\mathrm{straight}} = 12.516$. A large discrepancy can be noted between the skewed RTD predicted by the MTR model using that value (dashed orange line) in combination with variance parameter $k = 1-p$ and the measured RTD in a coiled tube of same diameter and length. This is to be expected as the conditions for a straight pipe fall in the middle of the transition regime as indicated by the magenta star in Fig. 1(a). To estimate the dispersion reduction factor κ for this case, we use a correlation of Florit et al. (2021) that was recently derived using CFD simulations. The authors distinguish between tight-coils and loose-coils and model κ as function of the Germano number (Ge) and the Schmidt number ($Sc = \nu/D$). For tight coils, as relevant here, it is $Ge \approx De$ where $De = Re\sqrt{d/2R_c}$ is the Dean number based on coil radius R_c. In the experiments of Gobert et al. (2017) it is $Sc \approx 520$. The tight-coils correlation of Florit et al. (2021) for the inverse dispersion reduction then factor becomes

$$\kappa^{-1} = 1 + 0.9415\left[\log_{10}\left(520De^2\right) - 2\right]^{1.983} \tag{58}$$

The value of the Dean number in the selected experiment of Gobert et al. (2017) is 11.2 resulting in $\kappa = 0.1195$ and $\alpha_{\mathrm{coiled}} = 1.496$. Fig. 10 shows that the RTDs of the MTR and dTiS models using that value are very similar to each other and agree quite well with the measured RTD. Given that this good agreement is obtained without any adjustment, the predictive capabilities of the MTR and dTiS models for coils are highlighted.

4.3. General reactors

Beside coil-based reactors, chip or plate-based reactors and packed bed reactors are widely used in continuous flow chemistry. Chip based reactors offer advantages in the wide range of geometries that can be manufactured including complex mixing sections while packed bed reactors are appropriate if heterogeneous catalysts or reagents are required. Traditional RTD analysis for characterization of these and other reactor types fits observed data from a pulse input or differentiated data from a step input to a model, such as AD or TiS. In this context, the variance is especially useful for matching experimental RTD curves to one of a family of theoretical curves. The long tails, however, often associated with the RTD measurements, distort variance values and yield fitting-parameter values of little accuracy. A Bodenstein number or other parameter computed in this way may be very much in error. This is because the later concentrations values of the recorded distributions normally cannot be determined with great accuracy but contribute heavily to the second moment (Ostergaard and Michelsen, 1969). Alternatively, RTD data can be fitted to theoretically calculated profiles and the "best fit" can be determined from the sum of squares of the differences between experimental and calculated values, an approach where one is not bothered by any long tail. Here, we demonstrate both concepts for the MTR and dTiS models using experimental RTD data for a flotation cell.

Guner et al. (2023) recently conducted a series of laboratory residence time measurements on the gas–liquid two-phase flow in a pneumatic flotation cell (Reflux™ RFC-100, cell volume 16 L). The authors studied six cases with different operating conditions, each case being

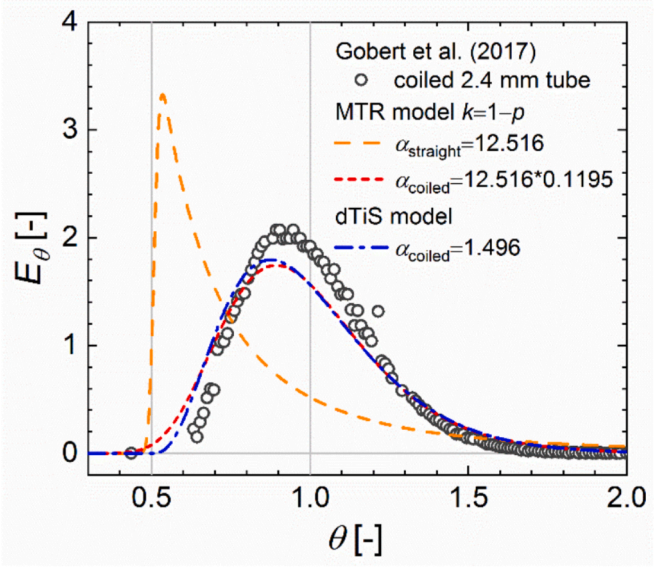

Fig. 10. Comparison of measured RTD data (Gobert et al., 2017) in a 2.4 mm coiled tube (symbols) with model predictions (lines). Predictions include the MTR and dTiS models for coiled tubes employing a dispersion reduction factor and the MTR model for a straight tube for comparison. The results of the MTR model are obtained in combination with $k = 1-p$.

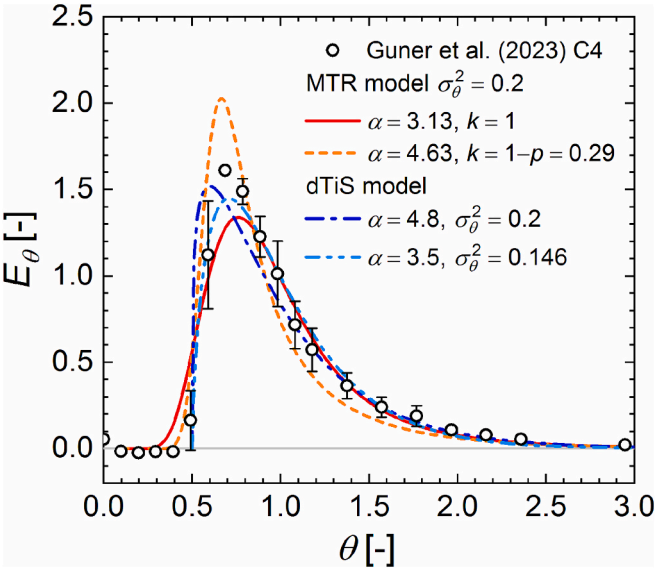

Fig. 11. Comparison of measured RTD in a pneumatic flotation cell (Guner et al., 2023) (symbols and error bars) with predictions by the MTR and dTiS models (lines) for reduced variance 0.2 and with least-squares fit of the dTiS model resulting in reduced variance 0.146.

repeated. Fig. 11 shows the RTD data of Guner et al. (2023, case C4) by symbols (open circles) and error bars. The authors did not report values for the RTD variance. However, their supplemental material provides all necessary information for calculation. For case C4, the reduced variance is estimated as $\sigma_\theta^2 = 0.20$ (see Supplemental Material, Section 4). The reduced variance of the dTiS model is $\alpha/24$ so that the effective time scale ratio is estimated as $\alpha = 4.8$. For the MTR model, the effective values of the time scale ratio are determined iteratively as 3.13 for $k = 1$ and as 4.63 for $k = 1-p = 0.29$. Fig. 11 shows that the MTR model with $k = 1$ underestimates the maximum of the experimental RTD, while the MTR model with $k = 1-p$ overestimates it. A better agreement is obtained with the dTiS model, though the position of the RTD maximum is shifted to lower values of θ. Despite the same value of the variance of 0.2, the three RTD curves differ notably. This illustrates the problem of determining the fitting parameter of models that have different tail behaviour from the measured variance when the tails of the RTD are truncated or affected by noise. A better agreement is obtained by a least-squares fit of the dTiS model to the experimental RTD as shown in Fig. 11, which yields $\alpha = 3.5$ and a reduced variance of 0.146. These results demonstrate that general reactors can be characterized by correlating the measured RTD by means of a weighted least-squares method applied to the MTR and dTiS models using α as fitting parameter.

5. Conclusions

Solute dispersion in a solvent flowing laminar through a pipe is of interest for continuous flow chemistry (CFC) and other fields. CFC is nowadays well established and widely used in a variety of industries and applications due to its efficiency, safety, and scalability. Solute dispersion arises by two competing processes. The axial transport of solutes by the non-uniform velocity field of the solvent creates radial concentration gradients, which tend to be eliminated by transverse diffusion. If the time scale of transversal diffusion is large as compared to the space time of the solvent streaming in Poiseuille flow, the dispersion and the associated RTD is described by the pure convection regime. If the time scale is small in contrast, the Taylor-Aris axial dispersion regime applies. Operation conditions in laminar tubular reactors as used in CFC often fall in the transition regime where neither longitudinal convection nor transversal diffusion are dominant and both, convection and diffusion determine dispersion and the RTD. In the transition regime, neither the pure convection nor the axial dispersion models are valid.

This paper uses a novel analytical approach to develop for solute transport in Poiseuille flow models for the RTD in the transition regime missing previously. Both proposed models yield continuous families of RTD curves that depend on a sole dimensionless parameter ($\alpha = Pe/4\lambda$), namely the ratio of transversal diffusion time to space time denoted as normalized transversal diffusion time. The mechanistic transition regime (MTR) model given by Eqs. (36), (42) and (54) is valid in the entire transition regime $0.25 < \alpha < 125$ and recovers the axial dispersion and pure convection models in the limits $\alpha \to 0.25$ and $\alpha \to 125$, respectively. A simpler phenomenological compartment model (dTiS) given by Eq. (55) is valid in the range $0.25 \le \alpha \le 6$. With increase of α, the RTD curves undergo a transition from the nearly symmetrical Gaussian shape typical for the axial dispersion regime towards the skew shape of the pure convection regime with sudden jump at the breakthrough time and long tails. To determine the normalized transversal diffusion time α, knowledge of the pipe diameter, pipe length, mean solvent velocity and molecular diffusivity of the solute is required. For applications in flow chemistry, α is usually known in advance to that the proposed models can be used to *predict* the RTD in straight tubes and, in combination with a dispersion reduction factor, also in coiled tubes as shown. The proposed models are furthermore useful to characterize skew RTDs occurring in other applications via the measured variance of the RTD or by a-posteriori fitting, as demonstrated for gas–liquid two-phase flow in a lab-scale pneumatic flotation cell.

In summary, the proposed models are the first developed specifically for the transition regime. They are predictive for straight and coiled tubes and can be used for reaction engineering design. They are also useful to predict or characterize RTDs in non-tubular reactors. Mathematical modeling can be further extended by combining RTD theory with chemical reaction kinetics to forecast conversion and yield.

Notation

Roman	
a	*Inner pipe radius, m.*
A	*Cross-section area of the pipe, $A = \pi a^2$, m^2.*
Bo	*Bodenstein number, $Bo = LU/D_{ax}$, dimensionless.*
c	*Solute (tracer) concentration, mol/m^3.*
c_{ref}	*Reference concentration, $c_{ref} = m/V_{reactor}$, mol/m^3.*
C	*Normalized tracer concentration, $C = c/c_{ref}$, dimensionless.*
d	*Inner pipe diameter, m/s.*
D	*Molecular diffusion coefficient, m^2/s.*
D_{ax}	*Axial dispersion coefficient, m^2/s.*
De	*Dean number, $De = Re\sqrt{d/2R_c}$, dimensionless.*
E	*Differential RTD, s^{-1}.*
E_θ	*Non-dimensional differential RTD, $E_\theta = \tau_s E$, dimensionless.*
F	*Cumulative RTD, dimensionless.*
Fo_d	*Fourier number, $Fo_d = \tau_s D/d^2 = 1/4\alpha$, dimensionless.*
$H(\bullet)$	*Heaviside function, dimensionless.*
k	*Variance parameter in MTR model, $k = 1$ or $k = 1-p$, dimensionless.*
L	*Axial distance between the tracer inlet and outlet planes, m.*
m	*Total amount of tracer/solute released in pulse input, mol.*
p	*Regime transition parameter of the MTR model, $0 < p < 1$, dimensionless.*
Pe	*Peclet number, $Pe = dU/D = Re{\cdot}Sc$, dimensionless.*
Q	*Volumetric flow rate of solvent, $Q = \pi a^2 U$, m^3/s.*
q	*Hypothetical number of tanks-in-series, dimensionless.*
r	*Radial coordinate, m.*
R	*Normalized radial coordinate, $R = r/a$, dimensionless.*
R_c	*Coil radius, m.*
Re	*Reynolds number $Re = dU/\nu$, dimensionless.*
S	*Model parameter related to variance of the MTR model, dimensionless.*
Sc	*Schmidt number $Sc = \nu/D$, dimensionless.*
t	*Time, s.*
$u(r)$	*Radial profile of axial velocity, m/s.*
U	*Mean axial velocity, m/s.*
U_{max}	*Maximum axial velocity, $U_{max} = 2U$, m/s.*
$V_{reactor}$	*Reactor volume, $V_{reactor} = \pi a^2 L$, m^3.*
$V(R)$	*Normalized axial velocity profile, $V = 2(1-R^2)$, dimensionless.*
z	*Axial coordinate, m.*
Z	*Normalized axial coordinate, $Z = z/L$, dimensionless.*
Greek	
α	*Normalized transversal diffusion time, $\alpha = \tau_d/\tau_s = a^2 U/LD$, dimensionless.*
α_{AD}	*Boundary between axial dispersion and transition regime, dimensionless.*
α_{PC}	*Boundary between pure convection and transition regime, dimensionless.*
$\Gamma(\bullet)$	*Complete Gamma function, $\Gamma(q) = \Gamma(q,0)$, dimensionless.*
$\Gamma(\bullet,\bullet)$	*Incomplete upper Gamma function, dimensionless.*
$\delta(\bullet)$	*Dirac delta function, dimension inverse to that of the argument.*
ε	*Small positive parameter, m.*
θ	*Normalized (reduced) time, $\theta = t/\tau_s = tU/L$, dimensionless.*
θ_f	*First appearance time, dimensionless.*
κ	*Dispersion reduction factor due coiling, $\kappa = D_{ax,coiled}/D_{ax,straight}$, dimensionless.*
λ	*Ratio between length and diameter of the circular pipe, $\lambda = L/d$, dimensionless.*
μ_n	*Moments of mixing cup concentration defined in Eq. (6), dimensionless.*
ν	*Kinematic viscosity of solvent, m^2/s.*
σ_θ^2	*Variance (around mean) of non-dimensional differential RTD, dimensionless.*
τ_s	*Space time, $\tau_s = V_{reactor}/Q = L/U$, s.*
τ_d	*Time scale of transversal diffusion, $\tau_d = a^2/D$, s.*
Acronyms.	
AD.	*Axial dispersion.*
CD.	*Convection dominated.*
CFC.	*Continuous flow chemistry.*
CSTR.	*Continuous stirred tank reactor.*
dTiS.	*Delayed-tank-in-series.*
MTR.	*Mechanistic transition regime (model)*
PC.	*Pure convection.*
PFR.	*Plug flow reactor.*
RT.	*Residence time.*
RTD.	*Residence time distribution.*
Averages	
$\widehat{(\bullet)}$	Cross-sectional area averaging operator defined in Eq. (11)
$\overline{(\bullet)}$	Time average

CRediT authorship contribution statement

Martin Wörner: Writing – review & editing, Writing – original draft, Visualization, Methodology, Investigation, Formal analysis, Conceptualization.

Funding

This research did not receive any specific grant from funding agencies in the public, commercial, or not-for-profit sectors.

Declaration of competing interest

The author declares that he has no known competing financial interests or personal relationships that could have appeared to influence the work reported in this paper.

Acknowledgements

The author thanks Jorge Gut, Sven Gobert and Leen Thomassen for providing the data of their publications (Dantas et al., 2014; Gobert et al., 2017).

Appendix A. Supplementary data

Supplementary data to this article can be found online at https://doi.org/10.1016/j.ces.2025.122116.

Data availability

Data will be made available on request.

References

Agar, D., et al., 2023. Roadmap chemical reaction engineering: an initiative of the DECHEMA/VDI subject division chemical reaction engineering. In: Gesellschaft für Chemische Technik und Biotechnologie (DECHEMA), 3rd ed. https://doi.org/10.5445/IR/1000165334

Ajdari, A., Bontoux, N., Stone, H.A., 2006. Hydrodynamic dispersion in shallow mirochannels: the effect of cross-sectional shape. Anal. Chem. 78, 387–392. https://doi.org/10.1021/Ac0508651.

Ananthakrishnan, V., Gill, W.N., Barduhn, A.J., 1965. Laminar dispersion in capillaries I. Mathematical analysis. Aiche J. 11, 1063–1072. https://doi.org/10.1002/aic.690110620.

Aris, R., 1956. On the dispersion of a solute in a fluid flowing through a tube. Proc. R. Soc. Lond. Ser. A-Math. Phys. Sci. 235, 67–77. https://doi.org/10.1098/rspa.1956.0065.

Aristizábal-Marulanda, V., Ramírez-Corona, N., Segovia-Hernández, J.G., 2024. Perspectives on sustainable processes in chemical engineering. In: Segovia-Hernandez, J.G., Ramírez-Corona, N., Aristizábal-Marulanda, V. (Eds.), Contributions of Chemical Engineering to Sustainability. Springer Nature, Switzerland, Cham, pp. 1–17. https://doi.org/10.1007/978-3-031-55594-7_1.

Atwood, J.G., Goldstein, J., 1984. Measurements of diffusion coefficients in liquids at atmospheric and elevated pressure by the chromatographic broadening technique. J. Phys. Chem. 88, 1875–1885. https://doi.org/10.1021/j150653a041.

Bailey, H.R., Gogarty, W.B., 1962. Numerical and experimental results on dispersion of a solute in a fluid in laminar flow through a tube. Proc. R. Soc. Lond. Ser. A-Math. Phys. Sci. 269, 352–367. https://doi.org/10.1098/rspa.1962.0182.

Bate, H., Rowlands, S., Sirs, J.A., 1973. Influence of diffusion on dispersion of indicators in blood-flow. J. Appl. Physiol. 34, 866–872. https://doi.org/10.1152/jappl.1973.34.6.866.

Bate, H., Rowlands, S., Sirs, J.A., Thomas, H.W., 1969. The dispersion of diffusible ions in fluid flow through a cylindrical tube. J. Phys. D-Appl. Phys. 2, 1447–1456. https://doi.org/10.1088/0022-3727/2/10/312.

Bhalode, P., Razavi, S.M., Roman-Ospino, A., Scicolone, J., Callegari, G., Tian, G., Koolivand, A., Krull, S., Ierapetritou, M.G., Muzzio, F.J., 2023. Optimal quantification of residence time distribution profiles from a quality assurance perspective. Int. J. Pharm. 634, 122653. https://doi.org/10.1016/j.ijpharm.2023.122653.

Bhalode, P., Tian, H., Gupta, S., Razavi, S.M., Roman-Ospino, A., Talebian, S., Singh, R., Scicolone, J.V., Muzzio, F.J., Ierapetritou, M., 2021. Using residence time distribution in pharmaceutical solid dose manufacturing – a critical review. Int. J. Pharm. 610, 121248. https://doi.org/10.1016/j.ijpharm.2021.121248.

Bharadwaj, R., Santiago, J.G., Mohammadi, B., 2002. Design and optimization of on-chip capillary electrophoresis. Electrophoresis 23, 2729–2744. https://doi.org/10.1002/1522-2683(200208)23:16<2729::Aid-Elps2729>3.0.Co;2-I.

Bischoff, K.B., McCracken, E.A., 1966. Tracer tests in flow systems. Ind. Eng. Chem. 58, 18–31. https://doi.org/10.1021/ie50679a005.

Bollini, P., Diwan, M., Gautam, P., Hartman, R.L., Hickman, D.A., Johnson, M., Kawase, M., Neurock, M., Patience, G.S., Stottlemyer, A., Vlachos, D.G., Wilhite, B., 2023. Vision 2050: reaction engineering roadmap. ACS Eng. Au 3, 364–390. https://doi.org/10.1021/acsengineeringau.3c00023.

Boskovic, D., Loebbecke, S., 2008. Modelling of the residence time distribution in micromixers. Chem. Eng. J. 135, S138–S146. https://doi.org/10.1016/j.cej.2007.07.058.

Bosworth, R.C.L., 1948. Distribution of reaction times for laminar flow in cylindrical reactors. Philos. Mag. Ser. 7 (39), 847–862. https://doi.org/10.1080/14786444808521811.

Bremer, J., Turek, T., 2024. From Bodenstein to Péclet - Dimensionless Numbers for Axial Dispersion in Chemical Reactors. Chem. Ing. Tech. 96, 1562–1569. https://doi.org/10.1002/cite.202400102.

Brenner, H., 1962. The diffusion model of longitudinal mixing in beds of finite length – numerical values. Chem. Eng. Sci. 17, 229–243. https://doi.org/10.1016/0009-2509(62)85002-7.

Brenner, H., 1990. Macrotransport processes. Langmuir 6, 1715–1724. https://doi.org/10.1021/la00102a001.

Buffham, B.A., Gibilaro, L.G., 1968. A generalization of tanks-in-series mixing model. AIChE J. 14, 805–806. https://doi.org/10.1002/aic.690140521.

Bursal, F.H., 1996. On interpolating between probability distributions. Appl. Math Comput. 77, 213–244. https://doi.org/10.1016/S0096-3003(95)00216-2.

Chatwin, P.C., Allen, C.M., 1985. Mathematical-models of dispersion in rivers and estuaries. Annu. Rev. Fluid Mech. 17, 119–149. https://doi.org/10.1146/annurev.fl.17.010185.001003.

Chen, Y.-C., Recanati, G., De Mathia, F., Lin, D.-Q., Jungbauer, A., 2024. Residence time distribution in continuous virus filtration. Biotechnol. Bioeng. 121, 1876–1888. https://doi.org/10.1002/bit.28696.

Colli, A.N., Bisang, J.M., 2015. Study of the influence of boundary conditions, non ideal stimulus and dynamics of sensors on the evaluation of residence time distributions. Electrochim. Acta 176, 463–471. https://doi.org/10.1016/j.electacta.2015.07.019.

Danckwerts, P.V., 1953. Continuous flow systems - distribution of residence times. Chem. Eng. Sci. 2, 1–13. https://doi.org/10.1016/0009-2509(53)80001-1.

Dantas, J.A.T.A., Pegoraro, P.R., Gut, J.A.W., 2014. Determination of the effective radial mass diffusivity in tubular reactors under non-Newtonian laminar flow using residence time distribution data. Int. J. Heat Mass Transf. 71, 18–25. https://doi.org/10.1016/j.ijheatmasstransfer.2013.12.003.

Datta, S., Ghosal, S., 2009. Characterizing dispersion in microfluidic channels. Lab Chip. 9, 2537–2550. https://doi.org/10.1039/b822948c.

Desmet, G., Broeckhoven, K., 2019. Extra-column band broadening effects in contemporary liquid chromatography: Causes and solutions. TrAC Trends Anal. Chem. 119, 115619. https://doi.org/10.1016/j.trac.2019.115619.

Ekambara, K., Joshi, J.B., 2004. Axial mixing in laminar pipe flows. Chem. Eng. Sci. 59, 3929–3944. https://doi.org/10.1016/j.ces.2004.05.025.

Emami Meibodi, M., 2022. Application of Axial Velocity Profile in Order to Develop Residence Time Distribution (RTD) for Different Laminar and Turbulent Flows. Iran. J. Chem. Chem. Eng. 41 (2), 493–500. https://doi.org/10.30492/ijcce.2020.135096.4290.

Erdogan, S., Wörner, M., 2013. Influence of channel cross-sectional shape on diffusion-free residence time distribution in fully developed laminar Newtonian flow. Chem. Eng. J. 227, 158–165. https://doi.org/10.1016/j.cej.2012.08.057.

Escotet-Espinoza, M.S., Moghtadernejad, S., Oka, S., Wang, Z., Wang, Y., Roman-Ospino, A., Schäfer, E., Cappuyns, P., Van Assche, I., Futran, M., Muzzio, F., Ierapetritou, M., 2019. Effect of material properties on the residence time distribution (RTD) characterization of powder blending unit operations. Part II of II: Application of models. Powder Technol. 344, 525–544. https://doi.org/10.1016/j.powtec.2018.12.051.

Farrell, M.A., Leonard, E.F., 1963. Dispersion in laminar flow by simultaneous convection and diffusion. AIChE J. 9, 190–195. https://doi.org/10.1002/aic.690090211.

Fazli-Abukheyli, R., Darvishi, P., 2019. Combination of axial dispersion and velocity profile in parallel tanks-in-series compartment model for prediction of residence time distribution in a wide range of non-ideal laminar flow regimes. Chem. Eng. Sci. 195, 531–540. https://doi.org/10.1016/j.ces.2018.09.052.

Florit, F., Rota, R., Jensen, K.F., 2021. Dispersion in coiled tubular reactors: a CFD and experimental analysis on the effect of pitch. Chem. Eng. Sci. 233, 116393. https://doi.org/10.1016/j.ces.2020.116393.

Gao, Y., Muzzio, F.J., Ierapetritou, M.G., 2012. A review of the Residence Time distribution (RTD) applications in solid unit operations. Powder Technol. 228, 416–423. https://doi.org/10.1016/j.powtec.2012.05.060.

Gibilaro, L.G., 1978. Residence time distribution for systems with open boundaries. Chem. Eng. Sci. 33, 487–492. https://doi.org/10.1016/0009-2509(78)80008-6.

Gill, W.N., 1967. A note on solution of transient dispersion problems. Proc. R. Soc. Lond. Ser. A-Math. Phys. Sci. 298, 335–339. https://doi.org/10.1098/rspa.1967.0107.

Gill, W.N., Ananthakrishnan, V., 1967. Laminar dispersion in capillaries: Part IV. The slug stimulus. Aiche J. 13, 801–807. https://doi.org/10.1002/aic.690130439.

Gill, W.N., Sankarasubramanian, R., 1970. Exact analysis of unsteady convective diffusion. Proc. R. Soc. Lond. Ser. A-Math. Phys. Sci. 316, 341–350. https://doi.org/10.1098/rspa.1970.0083.

Gobert, S.R.L., Kuhn, S., Braeken, L., Thomassen, L.C.J., 2017. Characterization of milli- and microflow reactors: mixing efficiency and residence time distribution. Org. Process Res. Dev. 21, 531–542. https://doi.org/10.1021/acs.oprd.6b00359.
Golay, M.J.E., Atwood, J.G., 1979. Early phases of the dispersion of a sample injected in poiseuille flow. J. Chromatogr. 186, 353–370. https://doi.org/10.1016/S0021-9673(00)95261-0.
Golbig, K., Kursawe, A., Hohmann, M., Taghavi-Moghadam, S., Schwalbe, T., 2005. Designing microreactors in chemical synthesis - Residence-time distribution of microchannel devices. Chem. Eng. Commun. 192, 620–629. https://doi.org/10.1080/00986440590495197.
Griffiths, D.A., Miller, A.J., 1973. Hyperbolic regression - a model based on two-phase piecewise linear regression with a smooth transition between regimes. Comm. Statist. Simulation Comput. 2, 561–569. https://doi.org/10.1080/03610927308827098.
Grimard, J., Dewasme, L., Vande Wouwer, A., 2016. A review of dynamic models of hot-melt extrusion. Processes 4, 19. https://doi.org/10.3390/pr4020019.
Guan, M., Chen, G., 2024. Streamwise dispersion of soluble matter in solvent flowing through a tube. J. Fluid Mech. 980, A33. https://doi.org/10.1017/jfm.2024.34.
Guidi, M., Seeberger, P.H., Gilmore, K., 2020. How to approach flow chemistry. Chem. Soc. Rev. 49, 8910–8932. https://doi.org/10.1039/C9CS00832B.
Guner, M.K., Hassanzadeh, A., Vinnett, L., Yianatos, J.B., Kowalczuk, P.B., 2023. Effects of operating parameters on residence time distribution in a REFLUX flotation cell. Miner. Eng. 204, 108439. https://doi.org/10.1016/j.mineng.2023.108439.
Gutierrez, C.G.C.C., Dias, E.F.T.S., Gut, J.A.W., 2010. Residence time distribution in holding tubes using generalized convection model and numerical convolution for non-ideal tracer detection. J. Food Eng. 98, 248–256. https://doi.org/10.1016/j.jfoodeng.2010.01.004.
Ham, J.-H., Lohse, R., Platzer, B., 2011. Modeling of the laminar flow in the entrance region of tubes and ducts and its impact on the residence time distribution. Chem. Ing. Tech. 83, 1245–1255. https://doi.org/10.1002/cite.201100004.
Hansen, E.H., Miró, M., 2007. How flow-injection analysis (FIA) over the past 25 years has changed our way of performing chemical analyses. TrAC-Trends Anal. Chem. 26, 18–26. https://doi.org/10.1016/j.trac.2006.07.010.
Hartman, R.L., Jensen, K.F., 2009. Microchemical systems for continuous-flow synthesis. Lab Chip 9, 2495–2507. https://doi.org/10.1039/B906343A.
Hereijgers, J., Breugelmans, T., de Malsche, W., 2015. Chromatography as an inspiration for microreactors. J. Chem. Technol. Biotechnol. 90, 2122–2131. https://doi.org/10.1002/jctb.4772.
Hessel, V., 2009. Novel process windows - gate to maximizing process intensification via flow chemistry. Chem. Eng. Technol. 32, 1655–1681. https://doi.org/10.1002/ceat.200900474.
Himmelblau, D.M., Bischoff, K.B., 1968. Process Analysis and Simulation: Deterministic Systems. Wiley, New York.
Holtze, C., Boehling, R., 2022. Batch or flow chemistry? – a current industrial opinion on process selection. Curr. Opin. Chem. Eng. 36, 100798. https://doi.org/10.1016/j.coche.2022.100798.
Hopley, A., Doyle, B.J., Roberge, D.M., Macchi, A., 2019. Residence time distribution in coil and plate micro-reactors. Chem. Eng. Sci. 207, 181–193. https://doi.org/10.1016/j.ces.2019.06.016.
Hsu, J.T., Dranoff, J.S., 1986. On initial condition problems for reactor dispersion model. Chem. Eng. Sci. 41, 1930–1934. https://doi.org/10.1016/0009-2509(86)87076-2.
Huang, Y., Seinfeld, J.H., 2019. A note on flow behavior in axially-dispersed plug flow reactors with step input of tracer. Atmos. Environ.: X 1, 100006. https://doi.org/10.1016/j.aeaoa.2019.100006.
Huber, D.E., Santiago, J.G., 2007. Taylor–Aris dispersion in temperature gradient focusing. Electrophoresis 28, 2333–2344. https://doi.org/10.1002/elps.200600830.
Huber, D.E., Santiago, J.G., 2008. Ballistic dispersion in temperature gradient focusing. Proceedings of the Royal Society A: Mathematical, Physical and Engineering Sciences 464, 595-612, doi: 10.1098/rspa.2007.0161.
Hubert, J., 1970. Effect of injection speed on the tracer concentration curves. Nukleonika 15, 52–57.
Janssen, L.A.M., 1976. Axial-dispersion in laminar-flow through coiled tubes. Chem. Eng. Sci. 31, 215–218. https://doi.org/10.1016/0009-2509(76)85059-2.
Jiang, W., Chen, G., 2018. Solution of Gill's generalized dispersion model: Solute transport in Poiseuille flow with wall absorption. Int. J. Heat Mass Transf. 127, 34–43. https://doi.org/10.1016/j.ijheatmasstransfer.2018.07.003.
Johnson, J.L., Fan, L.-T., Wu, Y.-S., 1971. Comparison of moments, S-plane, and frequency response methods for analyzing pulse testing data from flow systems. Ind. Eng. Chem. Process Des. Dev. 10, 425–431. https://doi.org/10.1021/i260040a001.
Kolev, S.D., 1995. Mathematical modelling of flow-injection systems. Anal. Chim. Acta 308, 36–66. https://doi.org/10.1016/0003-2670(94)00574-6.
Kolev, S.D., van der Linden, W.E., 1991. Laminar dispersion in parallel plate sections of flow systems used in analytical chemistry and chemical engineering. Anal. Chim. Acta 247, 51–60. https://doi.org/10.1016/S0003-2670(00)83051-2.
Korenaga, T., Shen, F., Takahashi, T., 1989a. An experimental-study of the dispersion in laminar tube flow. AIChE J. 35, 1395–1398. https://doi.org/10.1002/aic.690350821.
Korenaga, T., Shen, F.H., Yoshida, H., Takahashi, T., 1989b. Dispersion behavior of solutes in an ideal laminar-flow with small-bore glass tubes. Bull. Chem. Soc. Jpn. 62, 1492–1500. https://doi.org/10.1246/bcsj.62.1492.
Koutsky, J.A., Adler, R.J., 1964. Minimization of axial dispersion by use of secondary flow in helical tubes. Can. J. Chem. Eng. 42, 239–246. https://doi.org/10.1002/cjce.5450420602.
Kreft, A., Zuber, A., 1978. On the physical meaning of dispersion-equation and its solutions for different initial and boundary-conditions. Chem. Eng. Sci. 33, 1471–1480. https://doi.org/10.1016/0009-2509(78)85196-3.
Kreft, A., Zuber, A., 1979. Use of the dispersion model of fluid-flow. Int. J. Appl. Radiat. Isot. 30, 705–708. https://doi.org/10.1016/0020-708x(79)90113-3.
Levenspiel, O., 1999. Chemical Reaction Engineering, 3rd ed. John Wiley & Sons, Hoboken, NJ.
Levenspiel, O., 2012. Convection Model for Laminar Flow in Pipes. In: Levenspiel, O. (Ed.), Tracer Technology: Modeling the Flow of Fluids. Springer, New York, New York, NY, pp. 99–112. https://doi.org/10.1007/978-1-4419-8074-8_9.
Levenspiel, O., Lai, B.W., Chatlynne, C.Y., 1970. Tracer curves and the residence time distribution. Chem. Eng. Sci. 25, 1611–1613. https://doi.org/10.1016/0009-2509(70)85084-9.
Levenspiel, O., Smith, W.K., 1957. Notes on the diffusion-type model for the longitudinal mixing of fluids in flow. Chem. Eng. Sci. 6, 227–233. https://doi.org/10.1016/0009-2509(57)85021-0.
Levenspiel, O., Turner, J.C.R., 1970. Interpretation of residence-time experiments. Chem. Eng. Sci. 25, 1605–1609. https://doi.org/10.1016/0009-2509(70)85083-7.
MacMullin, R.B., Weber, M., 1935. The theory of short circuiting in continuous-flow mixing vessels in series and the kinetics of chemical reactions in such systems. Trans. Amer. Inst. Chem. Engrs 31, 409–458.
Martin, A.D., 2000. Interpretation of residence time distribution data. Chem. Eng. Sci. 55, 5907–5917. https://doi.org/10.1016/S0009-2509(00)00108-1.
Mayock, K.P., Tarbell, J.M., Duda, J.L., 1980. Numerical-simulation of solute-dispersion in laminar tube flow. Sep. Sci. Technol. 15, 1285–1296. https://doi.org/10.1080/01496398008068505.
Nagy, K.D., Shen, B., Jamison, T.F., Jensen, K.F., 2012. Mixing and dispersion in small-scale flow systems. Org. Process Res. Dev. 16, 976–981. https://doi.org/10.1021/op200349f.
Nauman, E.B., 1981. Residence time distributions and micromixing. Chem. Eng. Commun. 8, 53–131. https://doi.org/10.1080/00986448108912576.
Nauman, E.B., 2008. Residence time theory. Ind. Eng. Chem. Res. 47, 3752–3766. https://doi.org/10.1021/ie071635a.
Nechita, M.T., Suditu, G.D., Puitel, A.C., Dragoi, E.N., 2023. Residence time distribution: literature survey, functions, mathematical modeling, and case study-diagnosis for a photochemical reactor. Processes 11, 3420. https://doi.org/10.3390/pr11123420.
Osborne, F.T., 1975. Purely convective models for tubular reactors with non-newtonian flow. Chem. Eng. Sci. 30, 159–166. https://doi.org/10.1016/0009-2509(75)80001-7.
Ostergaard, K., Michelsen, M.L., 1969. On use of imperfect tracer pulse method for determination of hold-up and axial mixing. Can. J. Chem. Eng. 47, 107–112. https://doi.org/10.1002/cjce.5450470202.
Peng, Z., Brady, J.F., 2020. Upstream swimming and Taylor dispersion of active Brownian particles. Phys. Rev. Fluids 5, 073102. https://doi.org/10.1103/PhysRevFluids.5.073102.
Platzer, B., Steffani, K., Große, S., 1999. Möglichkeiten zur Vorausberechnung von Verweilzeitverteilungen. Chem. Ing. Tech. 71, 795–807. https://doi.org/10.1002/cite.330710805.
Plutschack, M.B., Pieber, B., Gilmore, K., Seeberger, P.H., 2017. The hitchhiker's guide to flow chemistry. Chem. Rev. 117, 11796–11893. https://doi.org/10.1021/acs.chemrev.7b00183.
Probstein, R.F., 1994. Physicochemical Hydrodynamics – An Introduction, 2nd ed. Butterworths, Boston.
Ratkowsky, D.A., 1990. Handbook of Nonlinear Regression Models. Dekker, New York.
Read, A.L., 1999. Linear interpolation of histograms. Nucl. Instrum. Methods Phys. Res., Sect. A 425, 357–360. https://doi.org/10.1016/S0168-9002(98)01347-3.
Reis, M.H., Varner, T.P., Leibfarth, F.A., 2019. The influence of residence time distribution on continuous-flow polymerization. Macromolecules 52, 3551–3557. https://doi.org/10.1021/acs.macromol.9b00454.
Rodrigues, A.E., 2021. Residence time distribution (RTD) revisited. Chem. Eng. Sci. 230, 116188. https://doi.org/10.1016/j.ces.2020.116188.
Rossi, D., Gargiulo, L., Valitov, G., Gavriilidis, A., Mazzei, L., 2017. Experimental characterization of axial dispersion in coiled flow inverters. Chem. Eng. Res. Des. 120, 159–170. https://doi.org/10.1016/j.cherd.2017.02.011.
Ruthven, D.M., 1971. Residence time distribution for ideal laminar flow in a helical tube. Chem. Eng. Sci. 26, 1113–1121. https://doi.org/10.1016/0009-2509(71)80025-8.
Sadriaj, D., Desmet, G., Cabooter, D., 2022. Taylor-Aris methodology for the experimental determination of molecular diffusion coefficients: Tutorial with focus on large biomolecules. J. Chromatogr. A 1664, 462787. https://doi.org/10.1016/j.chroma.2021.462787.
Sankarasubramanian, R., Gill, W.N., 1973. Unsteady convective diffusion with interphase mass transfer. Proc. R. Soc. Lond. A. Math. Phys. Sci. 333, 115–132. https://doi.org/10.1098/rspa.1973.0051.
Savage, T., Basha, N., McDonough, J., Krassowski, J., Matar, O.K., del Rio Chanona, E.A., 2024. Machine learning-assisted discovery of flow reactor designs. Nat. Chem. Eng. 1, 522–531. https://doi.org/10.1038/s44286-024-00099-1.
Saxena, A.K., Nigam, K.D.P., 1984. Coiled configuration for flow inversion and its effect on residence time distribution. AIChE J 30, 363–368. https://doi.org/10.1002/aic.690300303.
Schmalenberg, M., Krieger, W., Kockmann, N., 2019. Modular coiled flow inverter with narrow residence time distribution for process development and production. Chem. Ing. Tech. 91, 567–582. https://doi.org/10.1002/cite.201800172.
Shankar, A., Lenhoff, A.M., 1989. Dispersion in laminar-flow in short tubes. AIChE J 35, 2048–2052. https://doi.org/10.1002/aic.690351218.
Shankar, A., Lenhoff, A.M., 1991. Dispersion in round tubes and its implications for extra-column dispersion. J. Chromatogr. 556, 235–248. https://doi.org/10.1016/S0021-9673(01)96224-7.
Sharp, M.K., 1993. Shear-augmented dispersion in non-Newtonian fluids. Ann. Biomed. Eng. 21, 407–415. https://doi.org/10.1007/BF02368633.

Siguemoto, É.S., Leite Reche, L., Gut, J.A.W., Palma, M.S.A., 2020. Residence time distribution of a capillary microreactor used for pharmaceutical synthesis. Chem. Eng. Technol. 43, 429–435. https://doi.org/10.1002/ceat.201900478.

Spalding, D.B., 1958. A note on mean residence-times in steady flows of arbitrary complexity. Chem. Eng. Sci. 9, 74–77. https://doi.org/10.1016/0009-2509(58)87010-4.

Steffani, K., Platzer, B., 2002. Influence of velocity profile and diffusion on residence time distributions: mesoscopic modeling and application to Poiseuille flow. Chem. Eng. Process. 41, 143–155. https://doi.org/10.1016/S0255-2701(01)00124-6.

Stone, H.A., Stroock, A.D., Ajdari, A., 2004. Engineering flows in small devices. Annu. Rev. Fluid Mech. 36, 381–411. https://doi.org/10.1146/annurev.fluid.36.050802.122124.

Taylor, G.I., 1953. Dispersion of soluble matter in solvent flowing slowly through a tube. Proc. R. Soc. Lond. Ser. A-Math. Phys. Sci. 219, 186–203. https://doi.org/10.1098/rspa.1953.0139.

Taylor, G.I., 1954. Conditions under which dispersion of a solute in a stream of solvent can be used to measure molecular diffusion. Proc. R. Soc. Lond. Ser. A-Math. Phys. Sci. 225, 473–477. https://doi.org/10.1098/rspa.1954.0216.

Torres, A.P., Oliveira, F.A.R., 1998. Residence time distribution studies in continuous thermal processing of liquid foods: a review. J. Food Eng. 36, 1–30. https://doi.org/10.1016/S0260-8774(98)00037-5.

Trinidad, P., de Leon, C.P., Walsh, F.C., 2006. The application of flow dispersion models to the FM01-LC laboratory filter-press reactor. Electrochim. Acta 52, 604–613. https://doi.org/10.1016/j.electacta.2006.05.040.

Vanderslice, J.T., Stewart, K.K., Rosenfeld, A.G., Higgs, D.J., 1981. Laminar dispersion in flow-injection analysis. Talanta 28, 11–18. https://doi.org/10.1016/0039-9140(81)80131-2.

Vikhansky, A, 2011. Numerical analysis of residence time distribution in microchannels. Chem. Eng. Res. Des. 89, 347–351. https://doi.org/10.1016/j.cherd.2010.06.010.

Wang, X., Liu, Z., Pang, Y., 2017. Concentration gradient generation methods based on microfluidic systems. RSC Adv. 7, 29966–29984. https://doi.org/10.1039/C7RA04494A.

Wen, C.-J., Fan, L.-T., 1975. Models for Flow Systems and Chemical Reactors. Dekker, New York, NY.

Werner, T.M., Kadlec, R.H., 2000. Wetland residence time distribution modeling. Ecol. Eng. 15, 77–90. https://doi.org/10.1016/S0925-8574(99)00036-1.

Wibel, W., Wenka, A., Brandner, J.J., Dittmeyer, R., 2013. Measuring and modeling the residence time distribution of gas flows in multichannel microreactors. Chem. Eng. J. 215, 449–460. https://doi.org/10.1016/j.cej.2012.10.011.

Wissler, E.H., 1969. On applicability of taylor-aris axial diffusion model to tubular reactor calculations. Chem. Eng. Sci. 24, 527–539. https://doi.org/10.1016/0009-2509(69)85024-4.

Wörner, M., 2010. Approximate residence time distribution of fully develop laminar flow in a straight rectangular channel. Chem. Eng. Sci. 65, 3499–3507. https://doi.org/10.1016/j.ces.2010.02.047.

Wörner, M., 2015. General pure convection residence time distribution theory of fully developed laminar flows in straight planar and axisymmetric channels. Chem. Eng. Sci. 122, 555–564. https://doi.org/10.1016/j.ces.2014.10.015.

Young, W.R., Jones, S., 1991. Shear dispersion. Phys Fluids A-Fluid Dyn. 3, 1087–1101. https://doi.org/10.1063/1.858090.

Yu, J.S., 1976. Approximate analysis of laminar dispersion in circular tubes. J. Appl. Mech.-Trans. ASME 43, 537–542. https://doi.org/10.1115/1.3423925.

Zhang, B., Cui, Y., Shu, Y., Liao, B., Yang, M., Tang, C., 2024. Comparative analysis and selection criteria for residence time distribution models in free water surface constructed wetlands. J. Hydrol. 629, 130620. https://doi.org/10.1016/j.jhydrol.2024.130620.